Conservation of Dry Air, Water, and Energy in CAM and Its Potential Impact on Tropical Rainfall

BRYCE E. HARROP, MICHAEL S. PRITCHARD, HOSSEIN PARISHANI, ANDREW GETTELMAN, SAMSON HAGOS, PETER H. LAURITZEN, L. RUBY LEUNG, JIAN LU, KYLE G. PRESSEL, AND KOICHI SAKAGUCHI

^a Pacific Northwest National Laboratory, Richland, Washington
 ^b University of California Irvine, Irvine, California
 ^c National Center for Atmospheric Research, Boulder, Colorado

(Manuscript received 2 July 2021, in final form 16 November 2021)

ABSTRACT: For the Community Atmosphere Model version 6 (CAM6), an adjustment is needed to conserve dry air mass. This adjustment exposes an inconsistency in how CAM6's energy budget incorporates water—in CAM6 water in the vapor phase has energy, but condensed phases of water do not. When water vapor condenses, only its latent energy is retained in the model, while its remaining internal, potential, and kinetic energy are lost. A global fixer is used in the default CAM6 model to maintain global energy conservation, but locally the energy tendency associated with water changing phase violates the divergence theorem. This error in energy tendency is intrinsically tied to the water vapor tendency, and reaches its highest values in regions of heavy rainfall, where the error can be as high as 40 W m⁻² annually averaged. Several possible changes are outlined within this manuscript that would allow CAM6 to satisfy the divergence theorem locally. These fall into one of two categories: 1) modifying the surface flux to balance the local atmospheric energy tendency and 2) modifying the local atmospheric tendency to balance the surface plus top-of-atmosphere energy fluxes. To gauge which aspects of the simulated climate are most sensitive to this error, the simplest possible change—where condensed water still does not carry energy and a local energy fixer is used in place of the global one—is implemented within CAM6. Comparing this experiment with the default configuration of CAM6 reveals precipitation, particularly its variability, to be highly sensitive to the energy budget formulation.

SIGNIFICANCE STATEMENT: This study examines and explains spurious regional sources and sinks of energy in a widely used climate model. These energy errors result from not tracking energy associated with water after it transitions from the vapor phase to either liquid or ice. Instead, the model used a global fixer to offset the energy tendency related to the energy sources and sinks associated with condensed water species. We replace this global fixer with a local one to examine the model sensitivity to the regional energy error and find a large sensitivity in the simulated hydrologic cycle. This work suggests that the underlying thermodynamic assumptions in the model should be revisited to build confidence in the model-simulated regional-scale water and energy cycles.

KEYWORDS: Energy budget/balance; Climate models; General circulation models; Hydrologic cycle; Thermodynamics

1. Introduction

General circulation models are designed to directly simulate the large-scale motions of the atmosphere. Because processes such as turbulence, shallow and deep convection, microphysics, macrophysics, radiation, chemistry, and gravity waves (collectively referred to as the model physics) are important to these circulations and occur on scales smaller than the model grid spacing can resolve, they must be parameterized. Each parameterization acts to update the thermodynamic state of the model under an overarching set of imperfect assumptions that govern the model physics. For example, in the Community Atmosphere Model version 6 (CAM6), which is the atmosphere component of the Community Earth System Model version 2 (CESM2; Danabasoglu et al. 2020), a hybrid pressure system serves as the vertical coordinate for the model physics and the pressure at each model level is assumed to remain constant throughout the physics parameterizations (Neale et al. 2012). The constant

 ${\it Corresponding\ author}. \ Bryce\ E.\ Harrop, bryce.harrop@pnnl.gov$

hydrostatic pressure assumption used in CAM6 necessitates the use of a mass adjustment after the model physics have run to keep spurious sources and sinks of "dry" air (well-mixed, time-invariant gases like nitrogen, oxygen, and argon) from occurring. Lauritzen and Williamson (2019) showed that this mass adjustment has an associated energy tendency on the order of tens of watts per square meter. The goal of this work is to understand the energy tendency associated with the mass adjustment process and its impact on the simulated climate of CAM6.

It is known that a tendency in atmospheric column mass will result in a tendency in that column's energy, and this relationship has been examined in reanalyses (e.g., Trenberth 1997; Trenberth et al. 2002; Bosilovich et al. 2011). Studies of reanalyses tend to focus on mass perturbations brought about by the analysis increment, but there are also energy tendencies resulting from surface fluxes of water mass beyond latent heating. Indeed, Trenberth (1997) computes the energy tendency associated with a net surface water mass flux of 5 mm day⁻¹ as an energy flux of 15–17.5 W m⁻² (not including latent heat) depending on the vertically averaged moist static energy

DOI: 10.1175/JCLI-D-21-0512.1

(MSE) of the column. The energy tendency associated with surface mass fluxes has not received as much attention in free-running general circulation models. For example, a mass adjustment routine similar to that used in CAM6 was implemented into NASA's GEOS-5 model, yet the implications for the energy budget were not discussed (Takacs et al. 2016).

Understanding a model's energy budget is important for having confidence that the model simulations and projections are working for the right reasons, and it is also important to the broader community who make use of that model for analyses. In particular, there has been growing use of regional energy budgets as diagnostic or prognostic frameworks for understanding tropical rainfall patterns (Biasutti et al. 2018). Great success has been found in linking shifts of the intertropical convergence zone (ITCZ) to the cross-equatorial energy transport (e.g., Kang et al. 2009; Frierson et al. 2013; Adam et al. 2016), and recent work has also found success in extending that concept to explore meridional shifts of tropical rainfall (Boos and Korty 2016; Lu et al. 2021). As noted by Biasutti et al. (2018), despite successes as a diagnostic framework, the energetic framework suffers from limitations including the assumption that the circulations responsible for rainfall are energetically direct. In other words, these circulations diverge energy out of regions of heavy rainfall. Yet tropical rainfall regularly occurs in regions with shallow circulations where energy convergence is taking place (Back and Bretherton 2006; Inoue and Back 2017).

One aspect of the energy budget that was not considered in Biasutti et al. (2018) was the potential importance of terms neglected by making use of MSE as the conserved energy variable. Observations of enthalpy flux from rain over the tropical west Pacific suggest the enthalpy of rain can account for 15%-60% of the net surface heat flux for precipitation events, and over a 4-month period accounted for roughly 15% of the net surface heat flux (Anderson et al. 1998). Recent work by Mayer et al. (2017) showed that a more accurate depiction of the enthalpy of water, in particular condensed water species, has a nontrivial impact on regional surface energy exchanges estimated in reanalyses. Trenberth and Fasullo (2018) pointed out certain shortcomings with how Mayer et al. (2017) handled mass divergence, but they too found the energy flux associated with precipitation to be an important consideration for calculating energy budgets. One of the key results of the work of Mayer et al. (2017) and Trenberth and Fasullo (2018) is the need to use an energy budget that is consistent with the energy budget internal to the model being analyzed. Byrne and Schneider (2016) noted that it can be difficult to compute the flow of energy through the atmosphere directly from model output. As a result, they were forced to rely on the difference between the mean circulation and the net energy input to compute the eddy energy flux. Byrne and Schneider (2016) showed that this worked out well for one model they tested with higher-frequency output, but it may not work as well for all models. For example, when attempting to do something similar with output from CAM version 4, Harrop et al. (2019) needed to include the mass adjustment energy tendency found by Lauritzen and Williamson (2019) in

the net energy input component to accurately compute the total energy divergence by atmospheric motions.

In this work, we seek to bring together the above threads to better understand the mass adjustment energy tendency in CAM6. We will demonstrate that the adjustment energy tendency arises from CAM6's treatment of water in the energy budget; specifically, when water vapor in CAM6 condenses, only its latent energy is retained, while the remaining internal, potential, and kinetic energy that water vapor had is discarded. In the default CAM6 configuration, these spurious sources and sinks of energy associated with changes in water vapor mass are offset by their global mean value to preserve energy conservation on the global scale, but regionally these errors persist as the adjustment energy tendency. We will demonstrate how the adjustment energy tendency arises from the energy framework used by CAM6 in section 2, and we will also discuss the complications with how it is currently handled by the model. In section 3, we will explore potential pathways toward reconciling these issues. Finally, in section 4, we will examine a sensitivity test using CAM6 designed to gauge which aspects of the model are most sensitive to assumptions made in the thermodynamic budget. In section 5, we will summarize and discuss the findings of this article.

2. What is the mass adjustment process?

a. Why is an adjustment needed in CAM6?

We begin with a quick description of the CAM6 model used in this study. We use CAM6 from the release version of CESM2.1.0 (https://doi.org/10.5065/D67H1H0V). The model uses a nominal 1° regular latitude-longitude horizontal grid. We use the default dynamical core (i.e., primitive equation solver) for CAM6: the finite-volume dynamical core (Lin and Rood 1996, 1997). The physics parameterizations consist of the Cloud Layers Unified by Binomials (CLUBB) for the treatment of boundary layer turbulence, shallow convection, and macrophysics (Golaz et al. 2002; Bogenschutz et al. 2013), the Zhang-McFarlane treatment for deep convection (Zhang and McFarlane 1995), version 2 of the Morrison-Gettelman two-moment microphysics (MG2) for the treatment of cloud microphysics (Gettelman and Morrison 2015), the Rapid Radiative Transfer Model for GCMs (RRTMG) for the treatment of radiative transfer (Iacono et al. 2008; Mlawer et al. 1997), and the four-mode Modal Aerosol Module (MAM4) (Liu et al. 2016) for the treatment of aerosols. We run 16 years of an AMIP simulation (i.e., forced by prescribed, interannually varying sea surface temperatures) beginning in year 1979 using the default settings of CAM6. The first year of simulation is discarded as spinup, and the remaining years are averaged together to form a climatology of the simulation. Additional diagnostics were implemented in the model code base to add the ability to directly output the exact energy tendencies from the dynamical core and adjustment procedures separately from the rest of the physics.

In CAM6, parameterizations are "operator split" and most state variables (e.g., water vapor and temperature) are updated at the end of each parameterization. The CAM6 physics uses a hybrid sigma-pressure vertical coordinate system that is assumed to remain fixed throughout the individual parameterizations. Additionally, the model is assumed to be in hydrostatic balance, such that the pressure thickness of each model level is used to calculate the mass in that level. The mass of each level in CAM6 is the sum of dry air and water vapor (condensate mass is ignored). Treating the mass as the sum of dry air and water vapor is a reasonable approximation in many circumstances, but it means that as water transitions between the vapor and liquid or ice phases, the mass of the column can change, even if there is no flux of water across the surface. Since pressure is assumed to be constant during the physics calculations, the total mass (dry air plus water vapor) in each atmospheric layer is also unchanged during the physics. Assuming constant total mass (again, dry air plus water vapor) is a problem because parameterized water vapor mass changes imply changes to dry air mass, violating dry air mass conservation. To compensate for this dry mass conservation problem, an adjustment is made to the total mass to preserve dry air in each layer after all of the physics parameterizations have acted on the model state. The details of this adjustment process are presented in section 3.1.8 of Neale et al. (2012), but we reproduce the important pieces below to facilitate and motivate the work presented in this manuscript.

For a column in CAM6, the hydrostatic balance assumption means that

$$\frac{p_s}{g} = \frac{p_{\text{top}}}{g} + \sum_k \frac{\delta^k p}{g}$$

$$= \frac{p_{\text{top}}}{g} + \sum_k m_t^k$$

$$= \frac{p_{\text{top}}}{g} + \sum_k \left(m_d^k + m_v^k \right), \tag{1}$$

where p_s is the surface pressure, g is the gravitational acceleration (assumed to be a constant), $\delta^k p$ is the pressure thickness of level k, and m_t^k is the total mass of the layer (in units of kg m⁻²). CAM6 assumes the total mass, m_t^k , is the sum of dry air mass $\left(m_d^k\right)$ and water vapor mass $\left(m_v^k\right)$. The dry air mass and water vapor mass can equivalently be expressed in terms of pressure thickness and specific humidity as

$$m_d^k = \left(1 - q_v^k\right) \frac{\delta^k p}{\varrho},\tag{2}$$

$$m_v^k = q_v^k \frac{\delta^k p}{g},\tag{3}$$

where q_v^k is the specific humidity of level k, defined as $m_v^k/(m_d^k+m_v^k)$. Adopting the same notation as Neale et al. (2012), n is the time before the parameterizations have acted on the model state, n^* is the time after all parameterizations have run but before the adjustment, and n+1 is the time after the adjustment has been completed. The adjustment is formulated to conserve water vapor mass between times n^*

and n + 1, and dry air mass between times n and n + 1. Conservation is enforced at each model level such that

$$q_{v,n^*}^k \frac{\delta^k p_n}{g} = q_{v,n+1}^k \frac{\delta^k p_{n+1}}{g},$$
 (4)

$$(1 - q_{v,n}^k) \frac{\delta^k p_n}{g} = (1 - q_{v,n+1}^k) \frac{\delta^k p_{n+1}}{g}.$$
(5)

The above equations can be rearranged to get expressions for the pressure thickness and specific humidity after the adjustment:

$$\frac{\delta^k p_{n+1}}{g} = \frac{\delta^k p_n}{g} \left(1 - q_{v,n}^k + q_{v,n^*}^k \right), \tag{6}$$

$$q_{v,n+1}^k = \frac{q_{v,n}^k}{1 - q_{v,n}^k + q_{v,n}^k}. (7)$$

For the column mass, the change is

$$\frac{p_{s,n+1}}{g} = \frac{p_{\text{top}}}{g} + \sum_{k} \frac{\delta^{k} p_{n+1}}{g}$$

$$= \frac{p_{\text{top}}}{g} + \sum_{k} \frac{\delta^{k} p_{n}}{g} \left(1 - q_{v,n}^{k} + q_{v,n*}^{k} \right)$$

$$= \frac{p_{s,n}}{g} + \sum_{k} \frac{\delta^{k} p_{n}}{g} \left(q_{v,n*}^{k} - q_{v,n}^{k} \right), \tag{8}$$

which shows the new surface pressure is equal to the old surface pressure plus the column change in water vapor mass, as expected. Recall that in CAM6, only dry air and water vapor contribute to the hydrostatic pressure, so for a column with no change in dry air, the surface pressure change should equal the change in water vapor mass. Equation (7) can be rewritten for any model tracer (e.g., cloud liquid or aerosols) as

$$q_{x,n+1}^k = \frac{q_{x,n^*}^k}{1 - q_{v,n}^k + q_{v,n^*}^k},\tag{9}$$

where q_x is the tracer concentration. Note that the denominator is always the change in water vapor.

As expected, the column-integrated adjustment mass tendency balances the water vapor tendency. Averaged over long time scales, the adjustment mass tendency is nearly identical to the surface evaporation minus precipitation flux (E-P; see Fig. 1), which is balanced by the moisture convergence.

b. Why does the adjustment produce an energy tendency?

To understand the change in energy associated with the adjustment, it is useful to familiarize ourselves with the energy expression used by CAM6. CAM6 checks for energy conservation within the physics on a column-by-column basis. Because the model is assumed to be in hydrostatic balance,

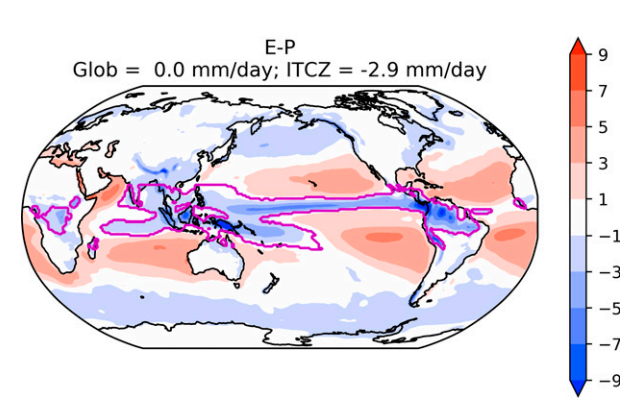


FIG. 1. Surface evaporation minus precipitation flux in units of mm day⁻¹. The magenta contour denotes the ITCZ region $(20^{\circ}\text{S}-20^{\circ}\text{N}, \text{where } P > 5 \text{ mm day}^{-1})$.

the following general expression for column-integrated energy is used (Williamson et al. 2015):

$$\varepsilon = \frac{1}{g} \sum_{k} \left[h^k + \frac{\left(u^k\right)^2 + \left(v^k\right)^2}{2} \right] \delta^k p + \frac{1}{g} p_s \Phi_s, \tag{10}$$

where ε is the column-integrated energy, h is the specific enthalpy, u and v are the zonal and meridional winds, and Φ_s is the surface geopotential. While Eq. (10) is what CAM6 aims to conserve, it is worth reminding readers that this representation with enthalpy and the surface geopotential term cannot be used to examine energy at an individual model level owing to the column integration being used in its derivation (see Kasahara 1974; Laprise and Girard 1990). It is also worth noting that there is no term related to $p_{\rm top}\Phi_{\rm top}$ because we are only interested in changes to the column energy and the model top is time-invariant. The expression for enthalpy used in CAM6 is

$$h = c_{nd}T + (L_v + L_f)q_v + L_fq_l, (11)$$

where c_{pd} is the specific heat at constant pressure for dry air, T is temperature, L_v and L_f are the latent heat of vaporization and fusion, respectively (both assumed constant), and q_l is the specific mass of liquid (both cloud and rain water). Combining Eqs. (10) and (11) gives

$$\varepsilon = \frac{1}{g} \sum_{k} \left[c_{pd} T^{k} + (L_{v} + L_{f}) q_{v}^{k} + L_{f} q_{l}^{k} + \frac{(u^{k})^{2} + (v^{k})^{2}}{2} \right] \delta^{k} p + \frac{1}{g} p_{s} \Phi_{s}.$$
 (12)

Equation (12) is the expression CAM uses in its internal energy checking algorithms. We refer to the $c_{pd}T$ term as the "thermal energy" term, the $(L_v + L_f)q_v + L_fq_l$ term as the "latent energy" term, the $0.5(u^2 + v^2)$ term as the "kinetic energy" term, and the $p_s\Phi_s/g$ term as the "potential energy" term. To better understand why the mass adjustment

produces an energy tendency, it is useful to rewrite Eq. (12) in terms of the layer mass using Eq. (1):

$$\varepsilon = \sum_{k} \left[c_{pd} \left(m_{d}^{k} + m_{v}^{k} \right) T^{k} + (L_{v} + L_{f}) m_{v}^{k} + L_{f} m_{l}^{k} + \left(m_{d}^{k} + m_{v}^{k} \right) \frac{(u^{k})^{2} + (v^{k})^{2}}{2} \right] + \sum_{l} \left(m_{d}^{k} + m_{v}^{k} \right) \Phi_{s}$$
(13)

Again, the p_{top} term is dropped because we are only interested in changes to column energy, ε . It is apparent from Eq. (13) that the mass of water vapor has thermal, potential, and kinetic energy (in addition to latent energy) in the CAM6 energy budget owing to the inclusion of its mass in the total mass used in the energy budget equation. The specific heat of dry air at constant pressure, c_{pd} , is used for both dry air and water vapor in CAM6, which is a point we will revisit in greater detail later in this manuscript. It is important to note again that the total mass (dry air plus water vapor) is assumed to be fixed during the physics parameterizations. In other words the sum of $m_d^k + m_v^k$ is held constant during the physics parameterizations and only updated during the adjustment process. Following the conservation restrictions in Eqs. (4) and (5), the adjustment update to total mass is equal to the change in water vapor mass during the physics ($\Delta m_{t,\text{adjustment}} = \Delta m_{v,\text{physics}}$). Therefore, we can write the change in energy owing to the adjustment as follows:

$$\Delta \varepsilon_{\text{adj}} = \sum_{k} \left[c_{pd} \Delta m_{v}^{k} T^{k} + \Delta m_{v}^{k} \frac{\left(u^{k}\right)^{2} + \left(v^{k}\right)^{2}}{2} \right] + \sum_{k} \left(\Delta m_{v}^{k}\right) \Phi_{s}, \tag{14}$$

where Δm_v^k is the net change in water vapor during the model physics, and can equivalently be thought of as Δm_t^k during the physics (since dry air mass is unchanged).

In Eq. (14) $\Delta \varepsilon_{\rm adj}$ is the change in column-integrated energy in CAM owing to the adjustment tendency and Δm_v^k is the water vapor mass change owing to the physics parameterizations, which is identically the total mass change required to conserve dry air mass during the adjustment. Thus, it is the inclusion of water vapor mass in the energy budget that gives rise to the adjustment energy tendency. Because water vapor has thermal, kinetic, and potential energy in the model, when water vapor is added or removed during the physics (e.g., through phase change), then thermal, kinetic, and potential energy is also added or removed.

The adjustment energy tendency can be seen in Fig. 2c. The energy tendencies related to the resolved dynamics, the physics parameterizations, and the residual are shown in Figs. 2a, 2b, and 2d, respectively. The adjustment energy tendency matches what was found by Lauritzen and Williamson (2019, their Fig. 7b). Even with accounting for the different color bars in Fig. 2, the adjustment tendency can be seen to be a nontrivial component of the regional energy budget. The

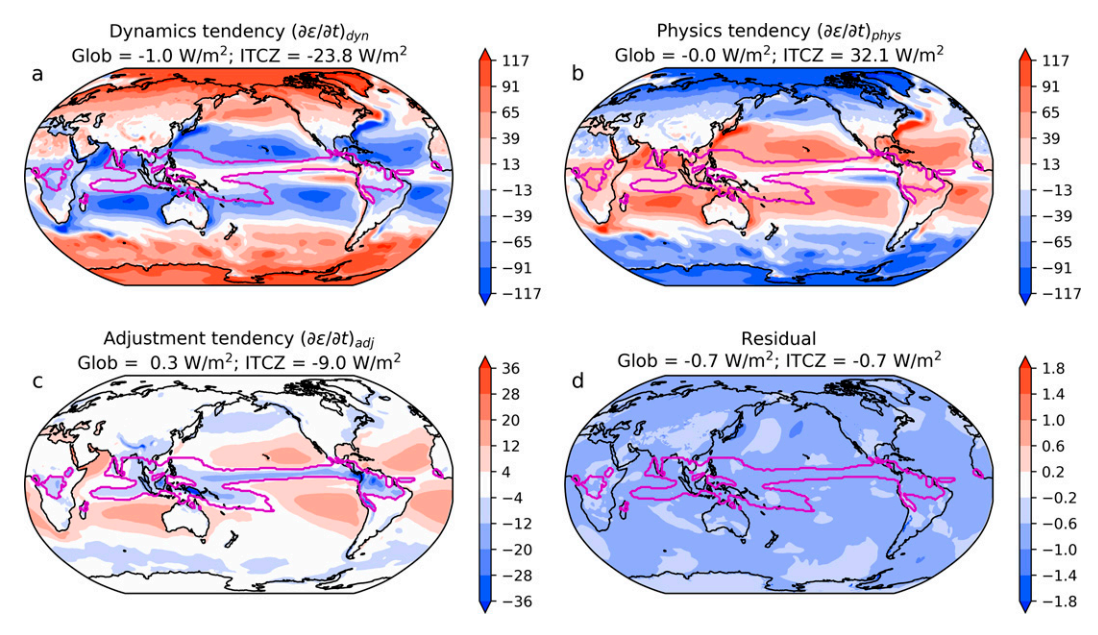


FIG. 2. Primary energy tendency terms for (a) dynamics, (b) physics, (c) adjustment, and (d) residual (energy fixer plus a time tendency owing to the disequilibrium of the atmosphere overlying an evolving SST pattern) taken from the CAM6 simulation. Units are W m⁻² for all panels. For the dynamics tendency, negative values indicate divergence of energy out of the region. Note that the color bar limits are not the same for each panel. The magenta contour denotes the ITCZ region ($20^{\circ}S-20^{\circ}N$, where P > 5 mm day⁻¹).

annual mean adjustment energy tendency follows the pattern of evaporation minus precipitation (cf. Figs. 1 and 2c) because this energy tendency is specifically tied to changes in water vapor.

c. Why is this an issue?

The key point from section 2b is that the adjustment energy tendency is the result of water vapor being included in the energy budget. Including water vapor in the mass used for the energy budget is not in itself a problem. In principle, the energy budget can be written with whatever constituents one likes, so long as the appropriate sources and sinks are accounted for in the model. The problem with CAM6 is that the appropriate sources and sinks are not being accounted for. The adjustment energy tendency in CAM6 is treated as an error that is handled globally by an energy fixer [for details on the fixer, see Neale et al. (2012)]. In other words, the adjustment energy tendency is averaged over the entire globe and that average is subtracted off of each atmospheric column. To illuminate this problem further, consider the following thought experiment. CAM6 has n columns and experiences condensation and precipitation in a single column, which has an adjustment energy tendency of $\Delta \varepsilon$. The energy tendency is globally averaged (assuming uniform area weights) to $\Delta \varepsilon / n$ and a counterbalancing offset is applied to each column. After this global offset, the column that formed precipitation still has an energy tendency, now equal to $\Delta \varepsilon [1 - (1/n)]$, and every other column now sees an energy tendency of $-\Delta \varepsilon / n$ even though those columns experience no change in water vapor. This scenario becomes even more problematic when one considers that CAM6 is often coupled

to other models such as land, ocean, and sea ice for climate and Earth system modeling. In a coupled system, one would expect the energy lost by water vapor condensation to be carried across the surface by precipitation. Instead, however, CAM6 assumes that hydrometeors have no energy and thus there is no surface energy flux associated with rain. This means that the divergence theorem, while satisfied globally because of the fixer, is violated locally for individual columns. We consider this local violation of the divergence theorem to be a significant problem given the magnitude of the regional adjustment energy tendencies (see again Fig. 2c). Constraints like the divergence theorem should be satisfied both locally and globally, if we are to increase confidence that the model simulated climate is working for the right reasons.

On top of violating the divergence theorem locally, the adjustment energy tendency is a nonnegligible part of the regional energy budget and, as such, adds a potential challenge for understanding the regional hydrologic cycle. As discussed in section 1, there has been growing interest in using the energy divergence by atmospheric motions to diagnose features related to the hydrologic cycle. The regional pattern of the adjustment energy tendency is a critical factor to

¹ The divergence theorem states $\iiint_V (\mathbf{\nabla} \cdot \mathbf{F}) dV = \oint_S \mathbf{F} \cdot \hat{n} \, dS$. For a volume with no internal sources or sinks of energy, $\partial \varepsilon / \partial t + \mathbf{\nabla} \cdot \mathbf{F}_\varepsilon = 0$. Combining this with the divergence theorem reveals that $\iiint_V (\partial \varepsilon / \partial t) dV = -\oint_S \mathbf{F}_\varepsilon \cdot \hat{n} \, dS$. In other words, the time tendency of the energy within the volume must equal the flux of energy into and out of the volume.

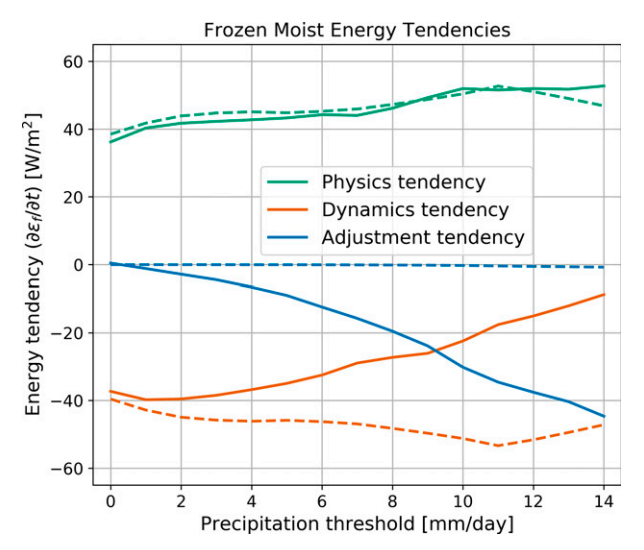


FIG. 3. Energy tendencies associated with the three dominant terms: physics, dynamics, and adjustment, for the frozen column energy [Eq. (15)]. Solid lines represent values for the default CAM6 configuration. Dashed lines represent the sensitivity experiment described in sections 3 and 4. All values are averaged over subregions within 20°S–20°N, wherein surface precipitation exceeds the precipitation threshold value given on the abscissa.

consider when attempting to apply these types of frameworks to CAM6. As an example, Fig. 3 shows the physics, dynamics, and adjustment frozen column energy tendencies averaged over the latitude range 20°S–20°N for different precipitation thresholds (shown on the abscissa). The frozen column energy is written as

$$\varepsilon_{\text{frzn}} = \frac{1}{g} \sum_{k} \left[c_{pd} T^{k} + L_{v} q_{v}^{k} - L_{f} q_{i}^{k} + \frac{\left(u^{k}\right)^{2} + \left(v^{k}\right)^{2}}{2} \right] \delta^{k} p + \frac{1}{g} p_{s} \Phi_{s}$$
(15)

and differs from the column energy in CAM6 only in the choice of enthalpy constants. Both are conserved equally well in CAM6. We opt to use the frozen column energy in Fig. 3 because it is comparable to the commonly used frozen moist static energy. It is worth pointing out here that the dynamics tendency is computed online within the model and is an accurate representation of the energy tendency resulting from the model's resolved dynamics. The physics tendency is the sum of radiative, sensible, and latent heating:

$$\frac{\partial \varepsilon_{\text{frzn}}}{\partial t}_{\text{physics}} = SW_{\text{net}} + LW_{\text{net}} + SHF + L_{v}E + L_{f}P_{s}, \quad (16)$$

where SW_{net} is the net SW heating, LW_{net} is the net LW heating, SHF is the sensible heat flux, E is the surface evaporation, and P_s is the surface snowfall.

Figure 3 shows the balance of the three energy terms is sensitive to the precipitation threshold chosen. Figure 3 also shows that as the averaging region is restricted toward higher rain rates, the adjustment energy tendency decreases as expected. The dynamics tendency, however, increases

(decreasing energy divergence) with increasing precipitation threshold. In other words, Fig. 3 suggests that in CAM6 energy divergence by the dynamics is weak for tropical regions with heavy rainfall, inconsistent with expectations from the energetic framework arguments for analyzing the hydrologic cycle. The physics tendency exceeds 40 W m⁻² for nearly all rain rates, but the balance of terms offsetting the physics tendency changes with precipitation threshold. When the precipitation threshold is zero (i.e., the entire 20°S–20°N region is horizontally aggregated), the adjustment tendency is roughly zero and there is balance between the physics and dynamics terms. At rain rates exceeding roughly 9 mm day⁻¹, the dynamics tendency is equal to the adjustment tendency and their sum balances the physics tendency.

3. How might we correct the energy error?

The regional energy error described in section 2c merits further discussion, particularly with an aim toward fixing the problem. In this section, we describe different paths toward remedying the regional energy error associated with the mass adjustment and weigh the pros and cons of each option. While this is not meant to be an exhaustive list, ultimately the surface flux and column energy tendency need to be brought into agreement with one another to satisfy the divergence theorem locally, so any solution will have some similarity to the suggestions described below.

To aid the discussion of the following proposed pathways, Fig. 4 summarizes the options discussed within this section. The default CAM6 version is shown at the top of the possible energy pathways for reference, and options A, B, C, and D correspond to sections 3a to 3d, respectively. In Fig. 4, each option is used to show what would happen to the energy associated with water vapor after it condenses and rains out.

a. Use adjustment tendency at surface

The first potential fix would be to remove the global fixer and prescribe a surface energy flux to match the adjustment energy tendency as it currently exists in CAM6. Using the adjustment energy tendency to compute a surface energy flux would guarantee the divergence theorem is upheld for the adjustment process. In Fig. 4, the remaining internal, kinetic, and potential energy of water vapor is transferred through the surface to other component models. This potential fix would also be relatively simple from the perspective of the atmosphere model, since minimal changes are needed. There are, however, many negative aspects of such a fix. First, there is no guarantee that changes to the other component models (land, ocean, and sea ice) would be similarly straightforward. For example, an increase in water vapor in the atmosphere has an energy tendency equivalent to adding water vapor at the temperature of the atmosphere, but the ocean or land models lose water vapor at the surface temperature. While these two temperatures are similar, they are not exactly equal and that difference can lead to energy conservation issues when the model is coupled. Second, it may not be possible to define a surface flux in regions where rain evaporates before reaching

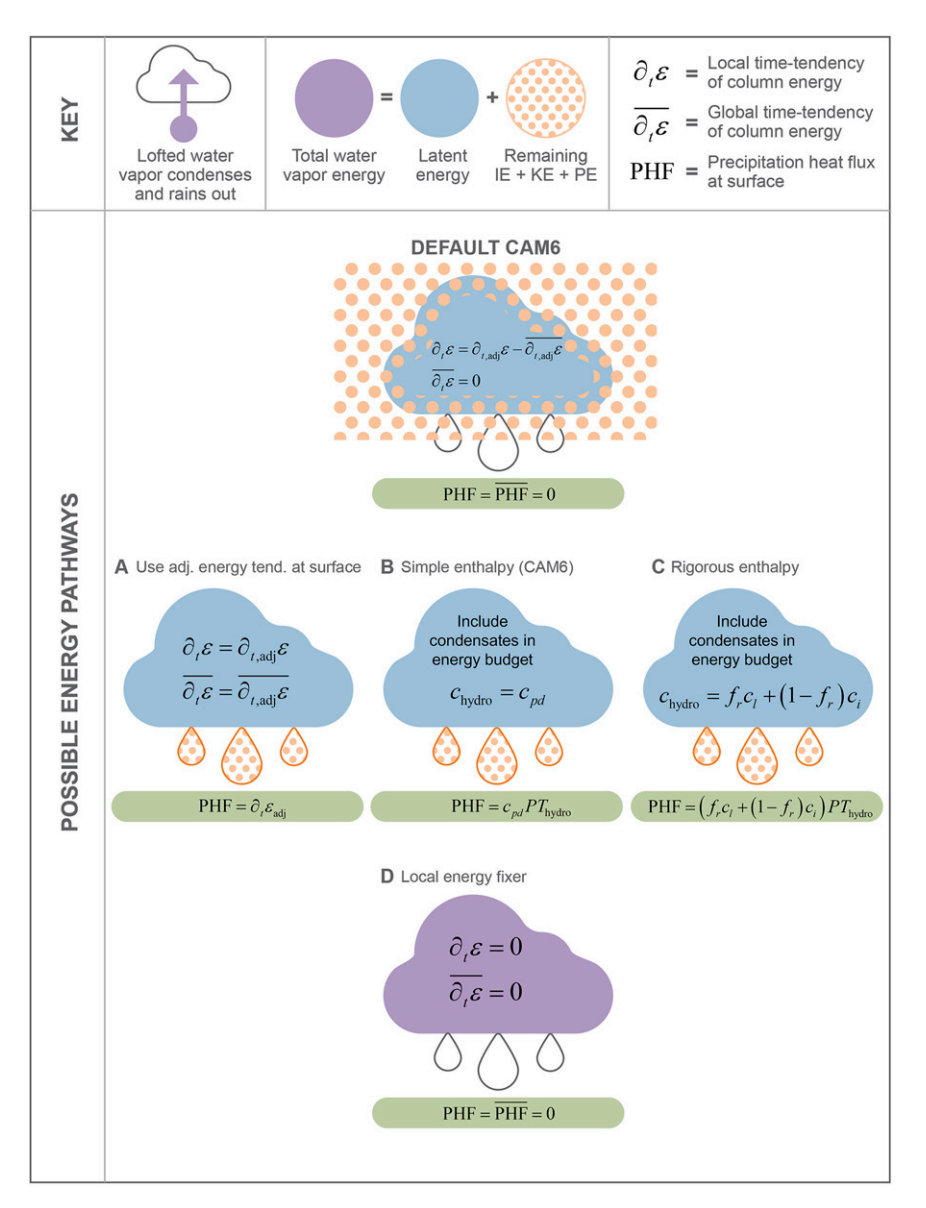


FIG. 4. Schematic example of energy pathways for the energy contained in water vapor that condenses and rains out. The default CAM6 method (described in section 2) is shown at the top. The alternative energy pathways proposed in this section are as follows: pathway A provides the adjustment energy tendency from Eq. (14) as a surface flux; pathway B include condensates in the energy budget, but continue to use the enthalpy expression currently in CAM6 [Eq. (11)]; pathway C is like B but uses a more rigorous expression for enthalpy; and pathway D assumes that condensates have no energy and all of the energy associated with water vapor is released during condensation (latent heat plus remaining internal, kinetic, and potential energy), i.e., it uses a local energy fixer. Here $c_{\rm hydro}$ refers to the specific heat of the hydrometeors, c_{pd} is the specific heat of dry air at constant pressure, c_l is the specific heat of liquid water, c_l is the specific heat of ice water, f_r is the fraction of hydrometeors in the liquid phase, P is the surface precipitation flux, and $T_{\rm hydro}$ is the temperature of the hydrometeors when they reach the surface.

the surface. For example, imagine some rain forming in the upper atmosphere at temperature T_1 , falling through the atmosphere, and then evaporating at temperature T_2 . From Eq. (14), there will be a change in thermal energy of $c_{pd}\Delta m_v^h(T_2-T_1)$. Physically, this energy tendency results

from the fact that the condensed water is no longer in equilibrium with the CAM6 atmosphere, so the temperature increase for the liquid water has no associated cooling from the remaining air. It is not ideal to prescribe a surface flux to handle processes that are inherently internal to the

atmosphere. Third, even when there is a surface precipitation flux, would setting its associated heat flux equal to the adjustment energy tendency produce physically plausible temperature values for the rain? As noted above, the rain is not being warmed by the atmosphere as it falls; whatever energy it has when it forms is the energy it would carry across the surface.

This third complication of whether the rain temperature values are realistic provides a nice segue into the surface enthalpy flux. To show the link between the rain temperature and surface enthalpy flux, we start with the expression for the surface enthalpy flux associated with water derived by Mayer et al. [2017, their Eq. (18)]. Since CAM6 uses a different expression for enthalpy than that derived in Mayer et al. (2017), we modify their surface enthalpy flux associated with water to be consistent with the assumptions made by CAM6. The appropriate surface enthalpy flux for water constituents in CAM6 would be

$$F_{\text{hw}} = \underbrace{c_{pd}ET_{\text{sfc}} - c_{pd}PT_{p}}_{\text{surface missing enthalpy flux}} + L_{s}E - L_{f}P_{\text{rain}}, \tag{17}$$

where F_{hw} is the surface enthalpy flux associated with water, E is the surface evaporation, $T_{\rm sfc}$ is the surface temperature, P is the surface precipitation, T_p is the temperature of precipitation, L_s is the latent heat of sublimation, L_f is the latent heat of fusion, and P_{rain} is the precipitation flux coming from liquid water only. In Eq. (17), the specific heats for all phases of water are set to the specific heat of dry air, c_{pd} , which follows from two assumptions made in CAM6's energy budget [Eq. (12)]. First, the mass of water vapor is not treated separately from dry air in Eq. (12), meaning it is consistent with the CAM6 framework to treat the specific heat of water vapor as equal to that of dry air. Second, CAM6 assumes constant latent heat values. Under Kirchoff's equations, this would suggest that all phases of water have the same specific heat. While this is obviously not true in the real world, in order to be consistent with the CAM6 energy budget, we must set the specific heats in Eq. (17) to be that of the dry air.

Equation (17) is valid under the assumptions made by CAM6, but it is not actually used in CAM6. Instead, only the last two terms on the right-hand side of Eq. (17) are computed in the model. The first two terms on the right-hand side of Eq. (17) $(c_{pd}ET_{sfc} - c_{pd}PT_p)$ are missing from the model, so for convenience we will refer to their combination as the surface missing enthalpy flux to distinguish it from the part of the surface enthalpy the model already computes. Our first proposed fix would be equivalent to setting the surface missing enthalpy flux equal to the adjustment energy tendency. Using the output from CAM6, we can estimate T_p under such an equality. When we do, we find the temperature difference between T_p and $T_{\rm sfc}$ to be on the order of tens of degrees. Averaged over the ITCZ region, defined here as the area within 20°S-20°N, where annual mean rainfall exceeds 5 mm day⁻¹, $T_p = 287.3$ K. Over the same ITCZ region, $T_{\rm sfc} = 300.5 \text{ K}$ —a difference from T_p of 13.2 K.

Observations and theory suggest the temperature of rain at the surface is nearly equal to the surface wet-bulb temperature (Byers et al. 1949; Kinzer and Gunn 1951; Gosnell

et al. 1995; Anderson et al. 1998; van Beek et al. 2012). The mean wet-bulb temperature [estimated using the numeric approximation of Stull (2011)] is 296.8 K—still a difference of nearly 10 K from our estimate of T_p when assuming the adjustment energy tendency can be used as the surface missing enthalpy flux. Therefore, simply treating the adjustment energy tendency as a surface energy flux that can be passed to other component models could result in unrealistic levels of surface cooling, depending on the level of thermodynamic complexity in the other component models.

b. Include condensates in energy budget

A potential fix that goes one step further than the one above would be to include the energy budget of hydrometeors as they fall through the atmosphere such that they can take up heat as they fall and reach the surface with a realistic temperature. We estimate such a budget offline using model outputs. Once water has condensed, it is no longer part of the column-integrated energy CAM6 uses [Eq. (12)]. Since we need to track the energy of the hydrometeors as they move through the column, we simply track the changes in internal, potential, and kinetic energy of the hydrometeors. The kinetic energy of hydrometeors is two to four orders of magnitude smaller than their internal and potential energy terms, so we will neglect it for this discussion. The internal energy change for the hydrometeors is simply the product of their specific heat, mass, and change in temperature. Similarly, the change in potential energy for the hydrometeors is the product of Earth's gravitational acceleration, mass, and change in altitude [Igel and Igel (2018) provide a derivation of the change in potential energy of hydrometeors]. At atmospheric pressures, $c_p = c_v$ for liquids and solids. To be consistent with CAM6, as noted above, we use c_{pd} for the specific heat of all water species. Thus, the changes in internal and potential energy can be written as

$$\Delta IE_{\text{hydro}} = c_{pd} m_{\text{hydro}} \Delta T, \qquad (18)$$

$$\Delta PE_{\text{hydro}} = g m_{\text{hydro}} \Delta z, \tag{19}$$

where ΔIE_{hydro} and ΔPE_{hydro} are the changes in hydrometeors' internal and potential energy, respectively, and m_{hydro} is the mass of the hydrometeors.

Equations (18) and (19) account for the changes in the hydrometeors' energy between where they form in the atmosphere and their energy when they reach the surface, which is a key piece to understanding the total atmospheric budget as noted by Trenberth and Fasullo (2018). These internal and potential energy budgets are computed simply as a diagnostic here. If the hydrometeors were able to interact energetically with the atmosphere, the change in internal energy would reflect the exchange of energy to bring the air and condensate into equilibrium (Romps 2008) and the change in potential energy would generate heat through frictional dissipation (Pauluis et al. 2000; Sabuwala et al. 2015; Igel and Igel 2018).

To make the calculations tractable using the CAM6 model output, we make the following assumptions. First, it is

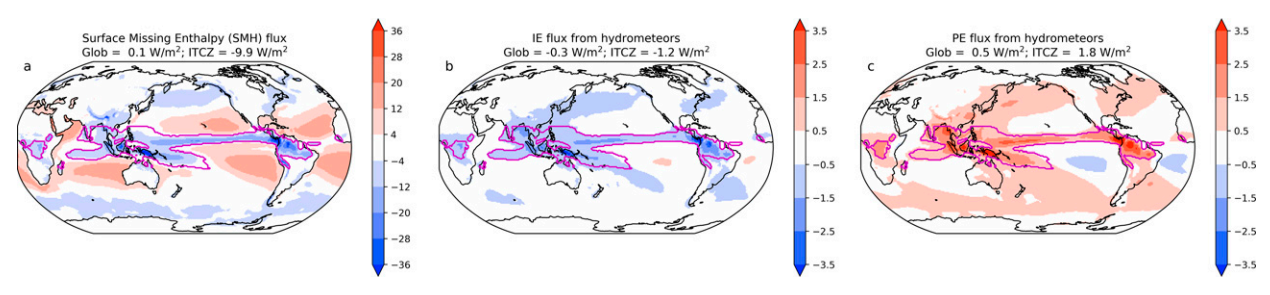


FIG. 5. (a) The surface missing enthalpy flux [thermal energy carried by water mass flux at the lower boundary of the atmosphere; bracketed part of Eq. (17)]. (b) Atmospheric cooling owing to warming of hydrometeors as they fall [vertical sum of Eq. (18)]. (c) Atmospheric warming owing to conversion of potential energy as hydrometeors fall [vertical sum of Eq. (19)]. All panels are in units of W m⁻². Note that the figure limits are not uniform across panels.

assumed that hydrometeors equilibrate to the actual temperature, not the wet bulb temperature. Byers et al. (1949) observed that as rain is falling the difference between the temperature and wet bulb temperature decreases, likely owing to the increasing relative humidity by drop evaporation. We apply this first assumption for both the calculation of the change in internal energy of hydrometeors as they fall through the atmosphere, as well as the calculation of their temperature at the surface. Second, the mass of hydrometeors falling through a layer is equal to the integrated water vapor physics tendency in the layers above. Neglecting the impact of cloud water remaining is reasonable because we are computing this budget using annual mean climatological tendencies. It is worth noting that using the net water vapor tendency means in places of net evaporation there are potential and internal energy tendencies associated with water vapor being fluxed into the atmosphere and mixed upward (this impacts more than just the lowest atmospheric level since vertical diffusion occurs in the model immediately after the surface fluxes are added). These tendencies associated with net evaporation, however, are much smaller than those associated with hydrometeors. Third, all condensation and evaporation occurs in an infinitesimal layer at the bottom of the model level. This third assumption means that condensation occurring in a model level does not contribute to frictional heating within that level. It also means that as rain falls into a level, the entire mass of water going into that level equilibrates to the temperature of that level, regardless of whether any evaporates.

We show the values of these budget terms in Fig. 5 evaluated from model outputs. Figures 5a-c show the energy tendencies and fluxes associated with water species [Eqs. (17)–(19), respectively]. The sign convention is that of the dry air perspective such that the internal energy term is negative because the air heats the hydrometeors as they fall (Fig. 5b), and the potential energy term is positive because the potential energy lost by the hydrometeors is converted to heat via friction (Fig. 5c). Estimates of the amount of potential energy lost to the atmosphere through frictional heating show it to range from approximately 2 to 5 W m⁻² in tropical rainfall regions (Pauluis et al. 2000; Pauluis and Held 2002; Romps 2008; Pauluis and Dias 2012; Igel and Igel 2018). Figure 5c shows that values tend to be on the low end of prior

estimates, but agreement is reasonable overall. The surface missing enthalpy flux is negative in regions of heavy precipitation because the water is carrying energy out of the atmosphere and giving it to the ocean or land (and vice versa in regions of net evaporation; Fig. 5a).

The first consequence is that the surface missing enthalpy flux is an order of magnitude larger than the other terms associated with the hydrometeors. Second, a lot of the frictional heating from the hydrometeors (the PE term in Fig. 5c) is offset by cooling from those hydrometeors. While not shown directly in Fig. 5, the sum of the surface missing enthalpy flux, internal energy, and potential energy terms shown in Fig. 5 does a remarkably good job of reproducing the adjustment energy tendency. The agreement is surprisingly good considering that the three terms [Eqs. (17)–(19)] were all computed offline using annual mean averages, and thus neglect covariances between temperature and rainfall on subannual time scales. The global mean difference between that sum and the adjustment energy tendency is only 0.06 W m⁻², their rootmean-square difference is 0.39 W m⁻², and their pattern correlation coefficient is 0.999.

Like in section 3a, the local divergence theorem is satisfied by including a surface flux to match the column energy tendency. The main difference between pathways A and B in Fig. 4 is that the hydrometeors are allowed to interact with the air as they fall. This allows for a realistic temperature of rainfall to be achieved at the surface, but it also means that the column energy tendency will not be the same as that of the adjustment energy tendency in the default CAM6 because of the IE and PE flux terms shown in Figs. 5b and 5c.

c. Include condensates and upgrade enthalpy

The most glaring drawback to the potential fix above is the use of c_{pd} for the specific heat in Eq. (18). The specific heat of liquid water is roughly 4 times larger than that of dry air, meaning it takes roughly 4 times as much energy to warm the same rain flux relative to our estimates above. No ocean model treats the enthalpy of liquid water using c_{pd} , so there will be an enthalpy flux mismatch when CAM6 is coupled to other models if the approach in section 3b is used. We can alleviate this issue by relaxing the assumption of constant latent heats for the enthalpy used in CAM6. Substituting a different expression for enthalpy that uses the

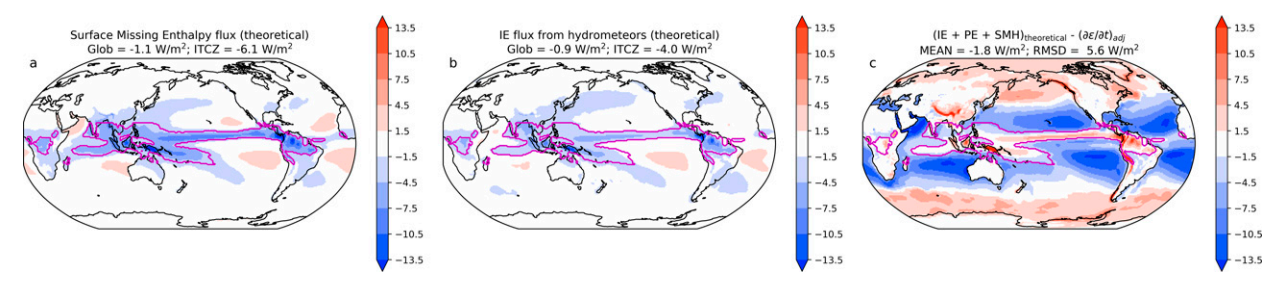


FIG. 6. (a),(b) As in Figs. 5a and 5b, but using the enthalpy formulation in Eq. (20). (c) The difference between the adjustment energy tendency and the sum of the internal energy, potential energy, and surface missing enthalpy flux terms. The mean and RMSD in (c) are both global values. All panels are in units of W m⁻².

correct specific heats of different phases of water provides a more realistic estimate of the potential falling hydrometeors have for cooling the atmosphere. The enthalpy expression we use is

$$h = [(1 - q_T)c_{pd} + q_{\nu}c_{p\nu} + q_lc_l + q_ic_i](T - T_R) + L_s(T_R)q_{\nu} + L_f(T_R)q_l,$$
(20)

where q_T is the total water mixing ratio $(q_v + q_l + q_i)$, c_{pv} is the specific heat at constant pressure for water vapor, c_l is the specific heat of liquid water, c_i is the specific heat of ice, and T_R is a reference temperature (taken to be 273.16 K). In Eq. (20), L_s and L_f are evaluated at the reference temperature, equivalent to the constant values used in CAM6. The derivation of Eq. (20) can be found in appendix A. Equation (20) is equivalent to the expression for enthalpy used by Mayer et al. (2017) up to a choice in constant.

Using Eq. (20), we formulate an expression for the surface missing enthalpy flux, as well as the internal and potential energy changes for hydrometeors. The total surface enthalpy flux from water that is consistent with Eq. (20) is

$$F_{\rm hw} = \underbrace{c_{pv}(T_{\rm sfc}-T_R)E - c_l(T_{\rm atm}-T_R)P_{\rm rain} - c_i(T_{\rm atm}-T_R)P_{\rm snow}}_{\text{surface missing enthalpy flux}}$$

$$+ L_s(T_R)E - L_f(T_R)P_{\text{rain}}. \tag{21}$$

By formulating the enthalpy expression to have latent heat terms using the reference temperature latent heat values, we cleanly separate the terms CAM6 calculates from those it currently neglects, which we continue to refer to as the surface missing enthalpy flux [denoted in Eq. (21)].

The surface missing enthalpy flux in Eq. (21) is a more rigorous treatment of the surface missing enthalpy flux than that in Eq. (17). The hydrometeor potential energy change [Eq. (19)] is not sensitive to the change in enthalpy formulation, but the hydrometeor internal energy change [Eq. (18)] is. For computing the internal energy difference, we replace c_{pd} in Eq. (18) with the specific heat for a condensate mixture, computed as

$$c_{\text{hvdro}} = f_r c_l + (1 - f_r) c_i,$$
 (22)

where f_r is the fraction of the total precipitation mass in the liquid phase.

Figure 6 shows the updated surface missing enthalpy flux (Fig. 6a) and internal energy term (Fig. 6b) using the enthalpy term in Eq. (20). The color scales differ between Figs. 5 and 6, but it is still clear that important differences exist. For convenience we will refer to the values computed using the enthalpy in Eq. (20) as the "theoretical enthalpy" and those using the enthalpy with assumed constant latent heat values in CAM6 as the "CAM6 enthalpy." For the surface missing enthalpy flux calculated using the CAM6 enthalpy, there is greater global cancellation between the evaporation regions and the precipitating regions than that using the theoretical enthalpy. Additionally, the energy losses from the atmosphere in the ITCZ region between the surface missing enthalpy flux and internal energy term are much more similar when using the theoretical enthalpy than when using the CAM6 enthalpy. Finally, Fig. 6c shows the difference between the sum of the three terms using the theoretical enthalpy and the adjustment energy tendency. Using the theoretical enthalpy estimate suggests the regional energy lost and gained from the atmosphere through the mass adjustment process is an overestimate, although direct comparison between different enthalpy estimates can be misleading owing to differences in the choice of constants and assumptions used.

The global and ITCZ mean values for the terms presented in Figs. 5 and 6 are summarized in Table 1. For the global mean, both the surface missing enthalpy flux and internal energy terms decrease in our theoretical estimate relative to what was computed using assumptions consistent with the current CAM6 energy budget. Instead of the sum of these missing terms heating the atmosphere in the global mean as

TABLE 1. All values diagnosed from the control simulation.

Field	Global mean	ITCZ mean
SMH flux (CAM6)	0.1	-9.9
SMH flux (theoretical)	-1.1	-6.1
IE flux (CAM6)	-0.3	-1.2
IE flux (theoretical)	-0.9	-4.0
PE flux	0.5	1.8
Sum (IE + PE + SMH; CAM6)	0.4	-9.3
Sum ($IE + PE + SMH$; theoretical)	-1.5	-8.3
Adjustment energy tendency $(\partial \varepsilon/\partial t)_{adj}$	0.3	-9.0

the CAM6 energy budget would suggest, the theoretical budget suggests these missing terms are a net cooling of -1.5 W m^{-2} to the atmosphere.

Recall that the above discussion stems from our desire to provide an appropriate surface flux for the adjustment energy tendency as a replacement for the global fixer to satisfy the divergence theorem. We outlined three options with increasing complexity and realism: 1) simply applying the adjustment energy tendency as a surface flux, 2) applying a surface enthalpy flux based on theoretical grounds for the enthalpy associated with water, but consistent with enthalpy used in CAM6, and 3) repeating option 2 with an enthalpy that allows for latent heats to vary with temperature. These three options are grouped together in Fig. 4 because all three relax the assumption that precipitation has no heat flux, and thus allow for a surface flux to balance the column energy tendency associated with water phase changes. Next, we will consider the opposite approach where we attempt to make the tendency within the atmosphere match the default CAM6 surface

d. Use a local energy fixer

An alternative option would be to continue to assume that condensed water species have no energy and that there is no surface enthalpy flux associated with water crossing the lower boundary of the atmosphere except for the latent heat term already computed in CAM6. In such a scenario the adjustment energy tendency currently offset by a global fixer would instead remain in the atmosphere locally. Physically, this would be as if the enthalpy of liquid and ice water were set to their reference enthalpy values $[L_t(T_R)]$ for liquid and 0 for ice]. For this case, condensation and deposition would result in a latent heating equivalent to the enthalpy of the water vapor that is lost, meaning it would not simply be the constant value used in CAM6. In other words, the temperature tendency would be larger for the same amount of condensation relative to the default CAM6 model. This difference in heating provided through condensation is shown schematically by comparing the default CAM6 and D pan-

Like in section 3a, this local fixer option results in an unphysical rainfall temperature (in this case, 0 K). For surface components that take rain temperature as an input, this unphysical rainfall temperature would result in erroneously large surface cooling. One could ask whether the use of an alternative reference temperature or enthalpy could alleviate the concern surrounding rainfall temperatures being too cold in the local fixer option. Since CAM6 assumes constant latent heats, the specific heat of water vapor, liquid, and ice are all equal, which, combined with the arbitrary nature of the reference enthalpy, means that the reference temperature is likewise arbitrary and its value can be freely chosen. The natural selection is to choose the reference temperature and enthalpy to match what is already used in CAM6. If one were to choose a different reference temperature, then there would be an additional surface flux term associated with that reference temperature [specifically, $c_{pd}(P - E)T_R$]. Attempting to

include that term in the local energy fixer would introduce a dependency of the local energy fixer on the reference temperature, which is not ideal. The optimal choice, again, is to use that which is already in CAM6 ($T_R = 0$ K).

It is straightforward to derive the temperature change needed to conserve enthalpy locally:

$$T_{n+1}^{k} = \frac{T_{n^*}^{k}}{1 - q_{nn}^{k} + q_{nn^*}^{k}}.$$
 (23)

The derivation of Eq. (23) is in appendix B. A similar equation is used to adjust the kinetic energy. As expected, Eq. (23) implies an increase in temperature for a decrease in water vapor $(q_{v,n}^k < q_{v,n}^k)$ via condensation or deposition.

Another possibility would be to reformulate the CAM6 energy to only consider dry air. For example, if CAM6 used a dry air pressure vertical coordinate there would be no need for the mass adjustment process and its associated energy tendency would vanish as well. From the analysis provided in section 2, assuming no other changes to the CAM6 energy framework (i.e., only changing m_t to be equal to m_d), this would be equivalent to letting water species in the atmosphere only have latent energy. For example, if water vapor were to condense and rain out, all of that latent heat would go into heating the dry air, and the falling hydrometeors would not carry any energy with them out of the atmosphere. Like the local conservation option above, this would also result in an increased temperature tendency for the same condensation owing to the fact that $m_d \leq m_t$.

e. Summary of energy error correction pathways

Any of the above options could be viewed as an improvement over the current method of applying a global fixer to cancel out the adjustment energy tendency. Updating the enthalpy expression used in CAM6 to better account for water across all phases is the most physically realistic option. Including the surface missing enthalpy flux terms was noted by Guo et al. (2019) to improve the seasonal cycle of equatorial Pacific SSTs, but reduces their interannual variability (using the NorESM1-F model—whose atmosphere model is a fork of CAM and has the same enthalpy definition as in CAM6).

An example of how to implement a rigorous enthalpy framework into a model was derived by Catry et al. (2007) and implemented into the AROME numerical weather prediction model by Degrauwe et al. (2016). Their results showed the largest consequences in scenarios with heavy rainfall. Implementing the Catry et al. (2007) framework or a similar one into CAM6 has the potential to be a major improvement for simulating the model climate, but is a technical challenge beyond the scope of the current work. Because CAM6 is frequently coupled to other components within CESM2, implementing the Catry et al. (2007) framework would require modifications to the other component models to conserve energy across the entire Earth system. Still, we think it is valuable for this work to run an experiment to gauge which aspects of the CAM6 simulated climate system are most

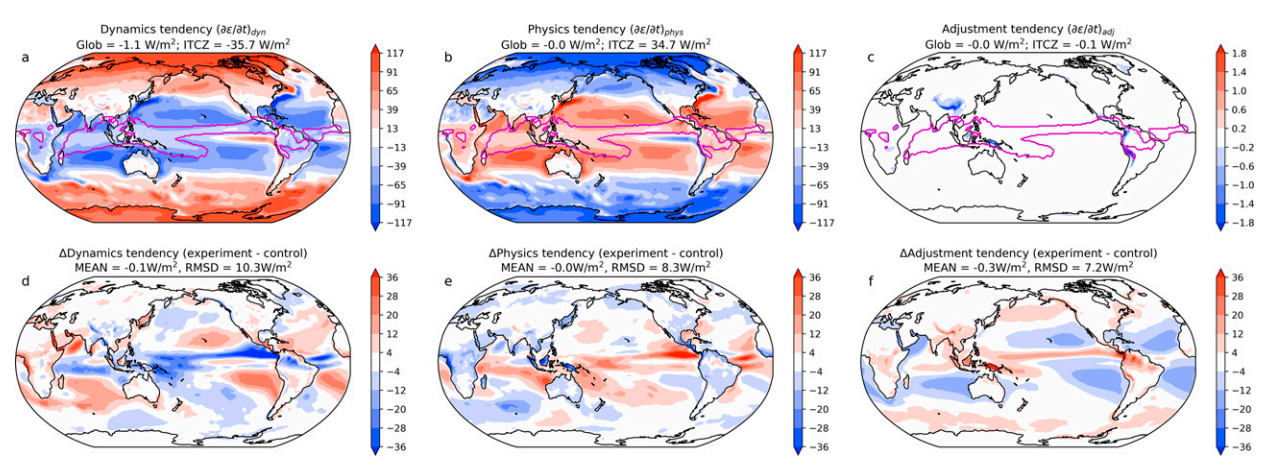


FIG. 7. (a)–(c) As in Figs. 2a–c, but using the experimental adjustment method. (d)–(f) Differences between (a)–(c) and the corresponding panels in Fig. 2.

sensitive to the assumptions made in the energy budget. With that in mind, we implement the option where the energy is fixed locally instead of globally. While we do not consider this option a fix because it continues to neglect the energy of condensed water species, it does give us a measure of how sensitive CAM6 is to the regional impact of the adjustment energy tendency. We explore this sensitivity test in the following section.

4. What impact does the adjustment energy tendency have on the simulated climate?

In this section, we will explore the sensitivity of CAM6 to the adjustment energy tendency. To do this, we run a sensitivity experiment to compare against the default configuration AMIP simulation discussed in the previous sections. As noted above, the sensitivity experiment is one where instead of applying a global fixer to offset the global mean adjustment energy tendency, we use a local energy fixer to offset the adjustment energy tendency in each column. It is important to stress that this experiment is not intended as a "fix" for CAM6, but instead is a simple test to gauge which aspects of the simulated climate system are most sensitive to the mass adjustment energy error. The local fix is done by modifying

temperature [via Eq. (23)] and winds such that the enthalpy and kinetic energy are conserved during the adjustment routine. We do not modify the surface geopotential to conserve the total column energy, but we show below that this term is small enough to ignore here.

We begin by comparing the energy tendencies (physics, dynamics, and adjustment) for the experiment relative to the control. Figure 7 shows that, as expected, the adjustment term goes to near-zero everywhere (note that the color limits for Fig. 7c are much smaller than those for Fig. 2c). Again, the adjustment tendency is not exactly zero because our formulation does not account for the $p_s\Phi_s/g$ term in Eq. (12). Thus, in regions where Φ_s is nonzero, there is still an energy tendency associated with the surface pressure change, especially near large topography. As can be seen in Fig. 7 and Table 2, however, this tendency is small and can be safely neglected for the analysis herein.

Figure 7 also shows the changes in the primary energy terms between the experiment and control. There are nontrivial signals in both the physics and dynamics tendency differences. These differences suggest that altering the treatment of energy carried by condensates in the dry mass adjustment procedure has a profound effect on the simulated climate state. The largest changes arise over the deep convective

TABLE 2. Simulated variables for the global mean of the control, experiment, and their difference (experiment minus control), as well as the ITCZ averaged region ($20^{\circ}\text{S}-20^{\circ}\text{N}$, where P > 5 mm day⁻¹) of the control, experiment, and their difference. For consistency with the model's energy formulation, LHFLX is equal to the last two terms on the right-hand side of Eq. (17).

Field	Global mean control	Global mean experiment	Global mean difference	ITCZ mean control	ITCZ mean experiment	ITCZ mean difference
$(\partial \varepsilon/\partial t)_{\text{phys}} (\text{W m}^{-2})$	-0.0	-0.0	-0.0	32.1	32.4	0.2
$(\partial \varepsilon/\partial t)_{\rm dyn} \ ({\rm W} \ {\rm m}^{-2})$	-1.0	-1.1	-0.1	-23.8	-33.4	-9.6
$(\partial \varepsilon / \partial t)_{\text{adj}} \text{ (W m}^{-2})$	0.3	-0.0	-0.3	-9.0	-0.1	8.9
Top-of-atmosphere net radiation (W m ⁻²)	4.0	-3.9	-7.9	68.6	61.1	-7.6
Longwave cloud radiative effect (W m ⁻²)	22.9	20.8	-2.1	44.6	36.8	-7.8
Shortwave cloud radiative effect (W m ⁻²)	-45.2	-49.5	-4.3	-64.9	-62.3	2.6
Latent heat flux (W m ⁻²)	84.9	87.9	3.1	104.1	114.5	10.4
Total surface precipitation (mm day ⁻¹)	2.9	3.0	0.1	6.9	7.6	0.7

regions of the tropics, particularly over the oceanic ITCZ region. We explore these impacts in greater detail below.

a. Energy from the global perspective

Reassuringly, the global mean energy tendencies for the physics are approximately zero in both the control and experiment (Table 2). The dynamical column energy tendency has a global error of roughly -1 W m^{-2} (it should be zero), and the adjustment tendency is roughly 0.3 W m⁻² (for the global mean) in the control and zero (as expected) in the experiment. The global mean values in the control simulation agree well with those shown in Table 1 of Lauritzen and Williamson (2019). The residual of the three primary energy terms is balanced by the model energy fixer: 0.7 W m⁻² for the control and 1.1 W m⁻² for the experiment (not shown). The fixer includes the offset needed to balance the global-mean adjustment tendency. The top-of-atmosphere radiation fluxes have a magnitude of about 4 W m⁻² globally, which is offset by an equal net surface flux to give the zero physics tendency terms (not shown). The difference in net TOA flux between the two experiments is -7.9 W m^{-2} , which is primarily driven by changes in the cloud radiative effects (SW + LW CRE = -6.4 W m^{-2}).

b. Energy from the ITCZ perspective

Over the ITCZ region, defined as the area of the tropics (20°S–20°N) where P > 5 mm day⁻¹, a fundamentally different balance of column energy tendencies occurs between the two simulations. At this regional scale, the individual energy tendencies have no constraint to be near zero, although they still sum to zero with the energy fixer. It is worth noting that the magnitude of regional energy fluxes is strongly tied to our arbitrary choice of enthalpy constants. For example, had we chosen the enthalpy to be zero for liquid instead of ice, all of the regional values would change. So long as we use a consistent enthalpy definition, however, we can still compare the regional flux of energy between the control and experiment. In both the control and the experiment the physics tendency—the net energy input to the atmosphere via radiative and turbulent heat fluxes—is about 32 W m⁻². In the control, the physics tendency is balanced by contributions from both the dynamics (convergence of energy by atmospheric motions) and the adjustment (removal of energy by hydrometeors). In the experiment, where the adjustment is near zero by design, the physics tendency is balanced by the dynamics alone. The fact that the physics tendency is roughly the same in both the control and the experiment implies that the energy sink associated with the adjustment term acts to reduce the divergence of energy by atmospheric circulations. That the energy divergence via atmospheric circulations is sensitive to the adjustment energy tendency is not surprising given that it is well known that atmospheric circulations are sensitive to heating within the tropical atmosphere (Hartmann et al. 1984; DeMaria 1985; Schumacher et al. 2004). What is surprising is that the whole of the response is in the change in the dynamics energy tendency. The physics, dynamics, and adjustment column-energy tendencies were also computed using the

enthalpy definition used by CAM6 (not shown) instead of the frozen column energy defined in Eq. (15), and while the values are different, the conclusions remain the same. The dynamics energy tendency response to the sensitivity experiment is much larger than that of the physics energy tendency.

The compensation between the adjustment energy tendency and the dynamics energy tendency is made even clearer looking again at Fig. 3. The dashed lines in Fig. 3 show the experiment. As expected, the adjustment energy tendency is zero regardless of precipitation threshold in the experiment, and the dynamics and physics tendencies balance one another. What is remarkable is the insensitivity of the physics tendency between simulations. When the atmosphere no longer loses energy via the adjustment energy tendency it diverges that energy away through atmospheric circulations. In short, the treatment of energy with respect to water (i.e., whether condensates are allowed to carry heat or not) fundamentally changes the way the modeled circulations redistribute energy within the tropical atmosphere.

c. Temperature and precipitation responses

Figure 8 shows warming across the global land surface in the sensitivity experiment relative to the control. Figure 8 also shows the 2-m air temperature biases over land compared to the Climate Research Unit (CRU) Global Climate Dataset temperature climatology for 1961-90 (Mitchell and Jones 2005; New et al. 1999). Since these experiments prescribe sea surface temperatures, there is very little near-surface temperature bias over the oceans. Figure 8 shows that with the new adjustment scheme there is an increase in temperature over land everywhere except eastern North America. We speculate that the warming over land results from removing the negative adjustment tendency over land, but there is also a slight increase in energy transport from ocean-to-land (about 4%; not shown) so remote influences cannot be ruled out either. An exact mechanism to explain this difference is beyond the scope of this work.

Figure 9 is the same as Fig. 8, but for the annual mean precipitation. Total precipitation increases along the equator, with decreases over the Amazon and Congo basins as well as over the Indian monsoon region. Global precipitation also increases, amplifying the global mean precipitation bias compared to the GPCPv2.2 data product (Adler et al. 2003) by roughly 50%. The global increase in rainfall suggests that the removal of energy by hydrometeors may dampen the overall hydrologic cycle, although this could change when that energy is coupled to other model components.

As an additional test that the sensitivities between the local and global fixer options (pathway D versus the default CAM6) are robust to a radical reformulation of parameterized physics, we compare the results against 10-yr simulations using a superparameterized version of SPCAM5 (Grabowski and Smolarkiewicz 1999; Grabowski 2001; Khairoutdinov and Randall 2001; Randall et al. 2003), which was configured like the default CAM6 but at 2° horizontal resolution. The superparameterized version of CAM

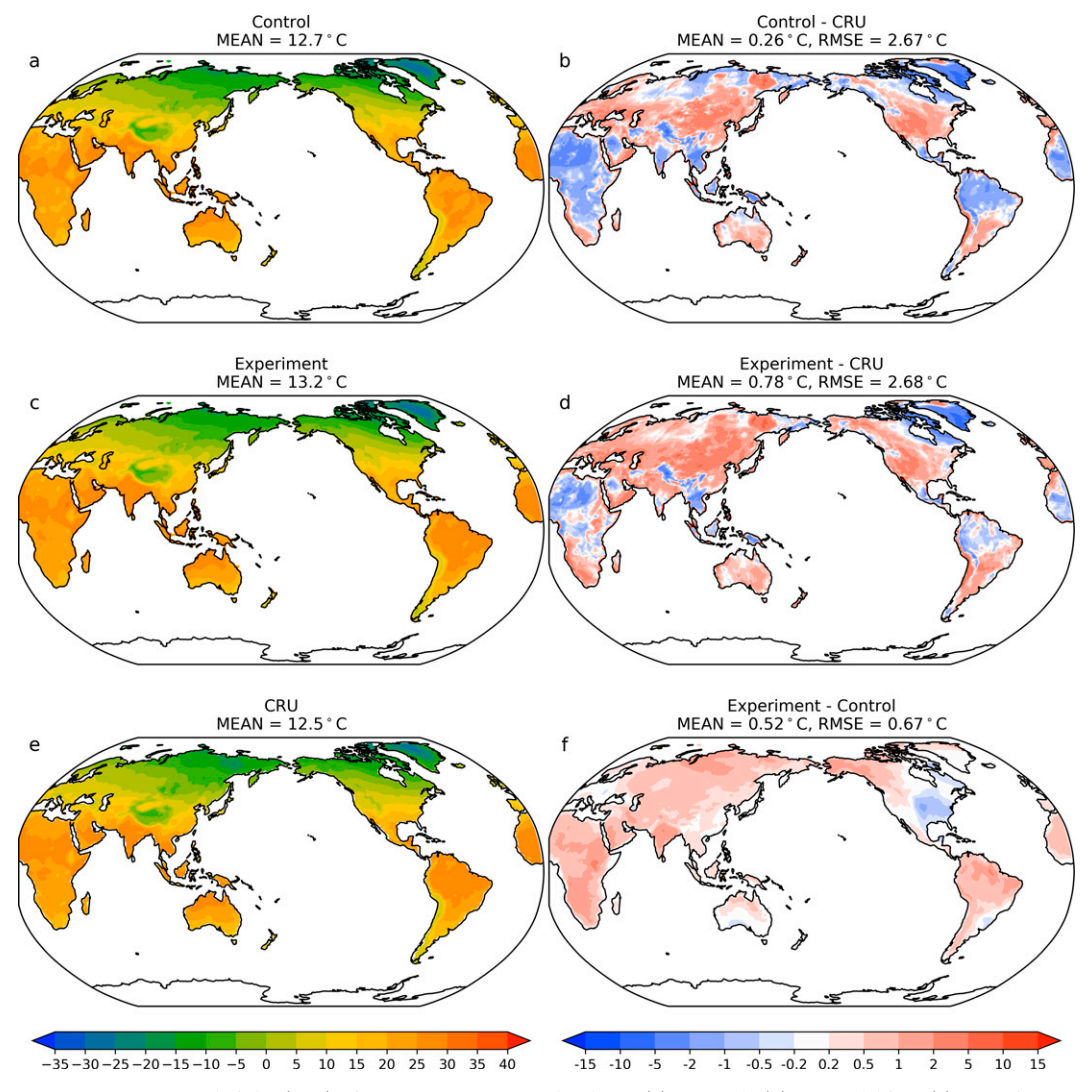


FIG. 8. Reference-height (2-m) air temperature over land for (a) control, (b) control bias, (c) experiment, (d) experiment bias, (e) observations (CRU), and (f) experiment minus control. Changes are minimal over oceans owing to the use of prescribed sea surface temperatures. Antarctica has been masked out to match the CRU dataset. Units are in °C.

replaces the convective and stratiform cloud parameterizations with embedded cloud-resolving models in each column of the host GCM. Figure 10 shows the rainfall response for both CAM6 with parameterized convection and for SPCAM with embedded cloud-resolving models. Despite dramatic differences in the baseline mean rainfall (cf. Figs. 10a and 10e), the response of the mean rainfall to the experimental adjustment is nearly identical between the two model configurations (Figs. 10b,f), confirming these are robust effects. Interestingly, not only does average precipitation increase near the equator, but the precipitation variance increases dramatically there as well. Figures 10d and 10h show the change in standard deviation of daily mean precipitation fluxes for the two sets of simulations. Like the mean rainfall response, the standard deviation change is similar for CAM6 and SPCAM. The resolved precipitation flux in

CAM6 dominates the increase in variance (not shown), suggesting an invigoration of convectively coupled wave dynamics may play a role.

The increase in convectively coupled wave activity is confirmed in Fig. 11 by contrasting the equatorial wave spectra across the simulations. The spectra were constructed following Wheeler and Kiladis (1999) to extract the equatorially symmetric component from daily anomalies of 15°S–15°N outgoing longwave radiation, using 96-day temporal window lengths overlapped by 20 days throughout the simulations (Wheeler and Kiladis 1999). It is immediately clear that there is a mode-selective variance boost in the moist Kelvin wave region of the spectrum in the sensitivity experiment relative to the control, both in the conventionally and superparameterized simulations. Preferential amplification of this buoyantly restored class of equatorial waves is consistent with the

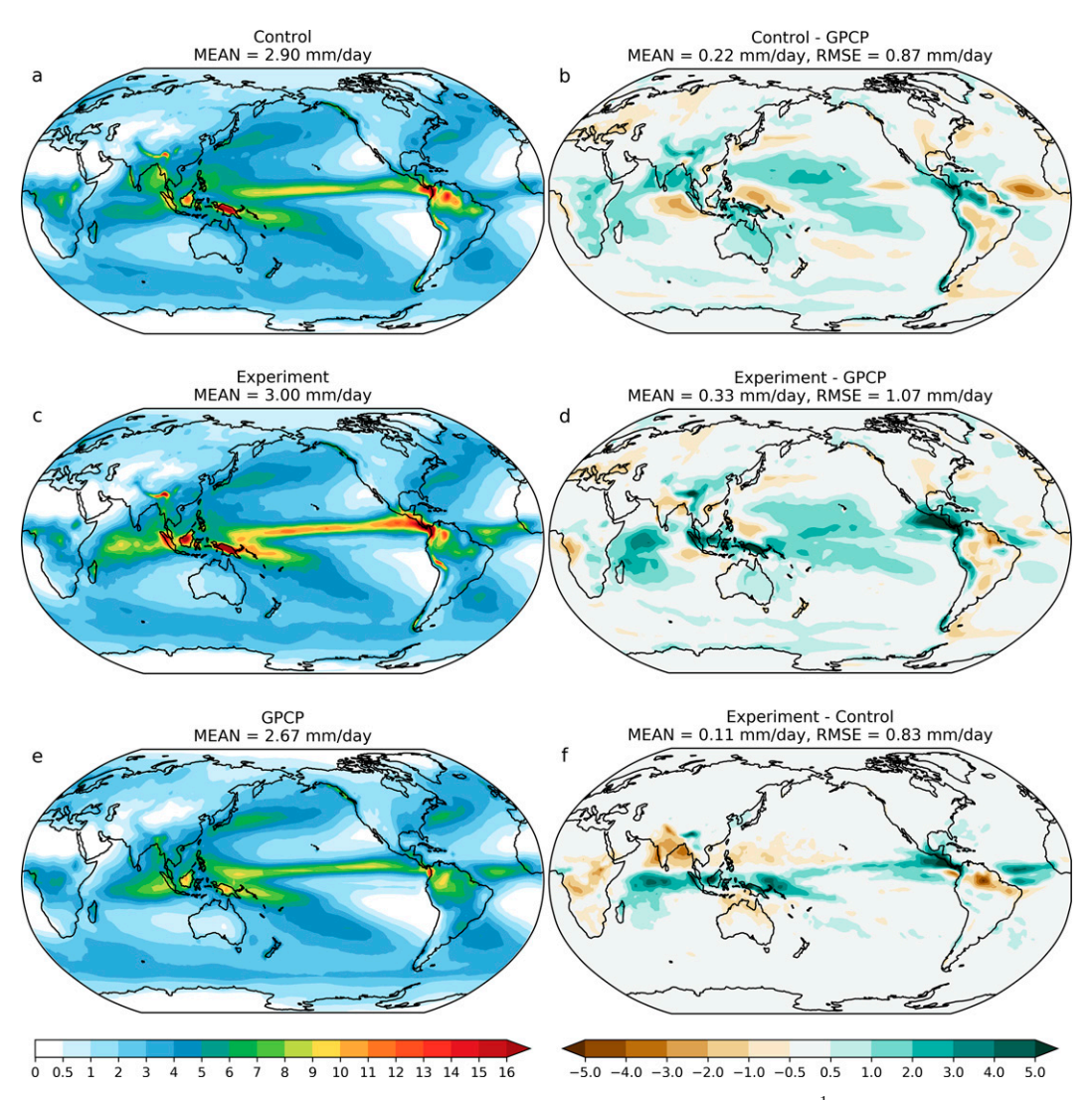


FIG. 9. As in Fig. 8, but for precipitation. Units are in mm day $^{-1}$.

increases in local temperature relative to the control when there is more condensation [Eq. (23)].

It is remarkable that the effects of the adjustment energy tendency on the wave spectrum in the baseline model (Fig. 11a vs Fig. 11b) are just as profound as the effects of superparameterization alone, including the emergence of a realistically dominant Madden-Julian oscillation (Fig. 11a vs Fig. 11c; Khairoutdinov et al. 2005; DeMott et al. 2007; Benedict and Randall 2009). Together with the effects noted in Fig. 10, this demonstrates that the assumptions made for the treatment of energy related to water species can have a large impact on the model hydrological cycle and especially equatorial wave dynamics. Our findings point to the conclusion that the increased temperature tendency from latent heating generates additional buoyancy within precipitating systems, creating favorable conditions for additional precipitation in the subsequent model time steps.

Figure 12 shows the rain rate amount distribution globally (Fig. 12a) and in the ITCZ region (Fig. 12b; where P > 5 mm day⁻¹ in the latitude range of 20°S–20°N). The amount distribution is computed following the methodology of Pendergrass and Hartmann (2014), where the bins have a 7% spacing and the minimum rainfall rate counted is 0.029 mm day⁻¹. The Global Precipitation Climatology Project One Degree Daily (GPCP 1DD; Huffman et al. 2001; Huffman and Bolvin 2013a,b) distribution is presented for reference. Note that the GPCP dataset has its own uncertainties owing to its reliance on cloud brightness temperature instead of direct rainfall measures. The Tropical Rainfall Measuring Mission (TRMM; Huffman et al. 2007), which includes measures from the TRMM Precipitation Radar, shows noticeable differences from GPCP in rainfall amount in the tropics (see Kooperman et al. 2016). The TRMM dataset compares favorably with SPCAM in the control configuration (Kooperman et al. 2016). For both the CAM6 and SPCAM experiments

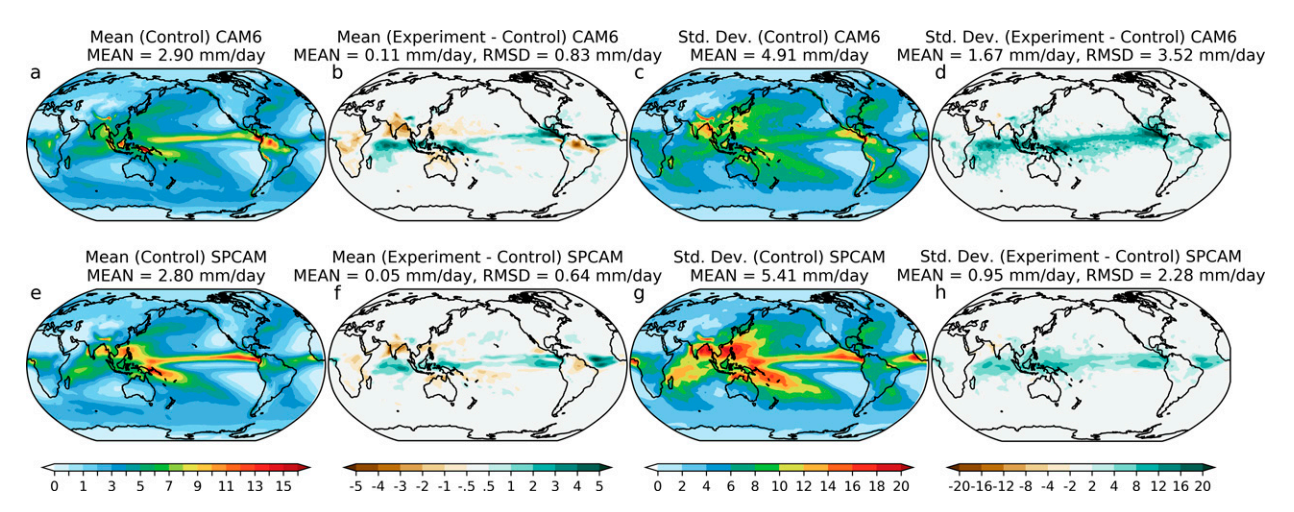


FIG. 10. Precipitation patterns and changes for (top) CAM6 and (bottom) SPCAM. (a),(e) The mean precipitation for the control simulations; (b),(f) the change in precipitation between the experiment and control; (c),(g) the standard deviation of daily precipitation for the control simulations; and (d),(h) the change in standard deviation of daily precipitation. All panels are in units of mm day $^{-1}$.

relative to their control simulations, there is a shift in the amount distribution toward more rainfall coming from heavy rain rate events both globally and throughout the ITCZ region. In both control simulations, there is very little rainfall coming from rain rates exceeding 100 mm day⁻¹, while in both experiment simulations these very heavy rain rates produce a significant portion of the total rainfall.

The change in the hydrological cycle is also apparent in the cloud fields, as seen by the cloud radiative effects. Figure 13a shows the LWCRE decreases across the tropics except in the regions of largest precipitation increase, consistent with a shift from more frequent, mild (parameterized) convection to less frequent, vigorous (resolved) convection (for CAM6). Additionally, the SWCRE increases (decreasing magnitude) over

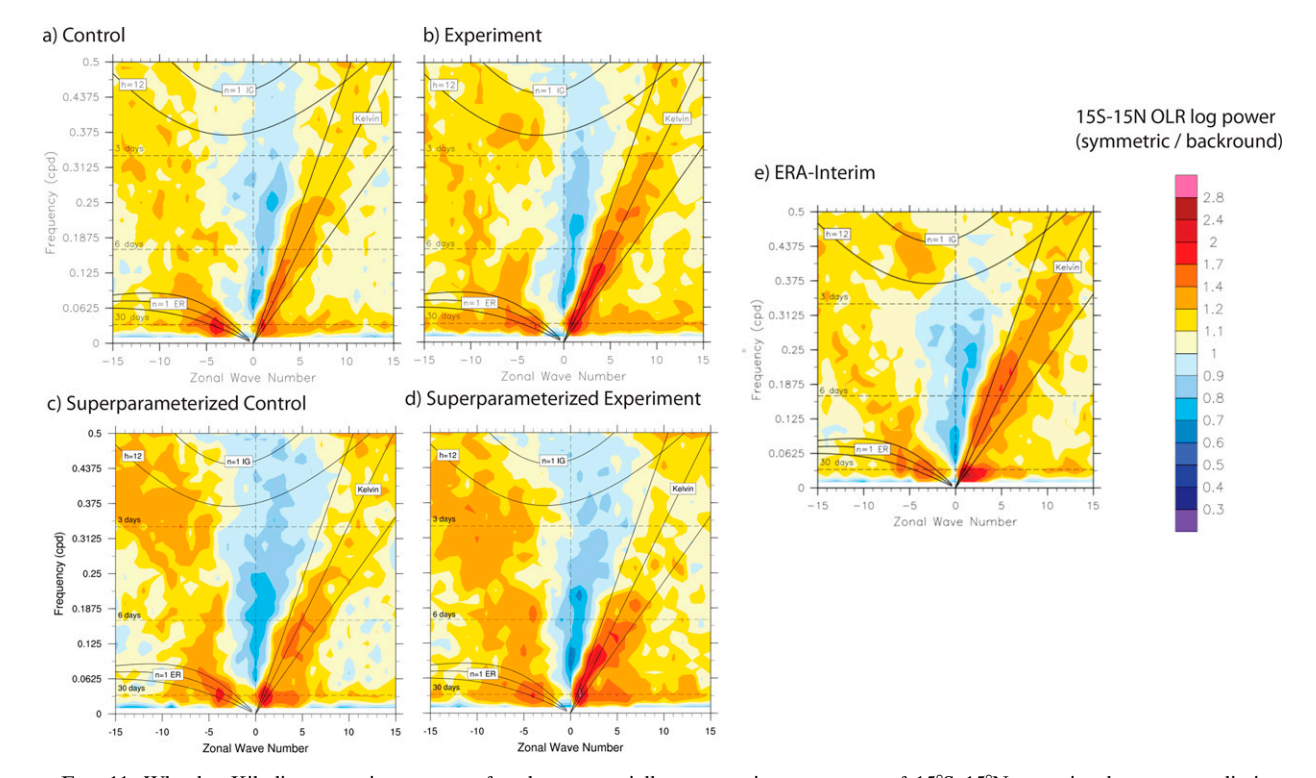


FIG. 11. Wheeler–Kiladis space–time spectra for the equatorially symmetric component of 15°S–15°N outgoing longwave radiation anomalies, comparing (left) control vs (right) experiment results in (a),(b) conventionally vs (c),(d) superparameterized versions of CAM. (e) Climatological benchmark from ERA-Interim.

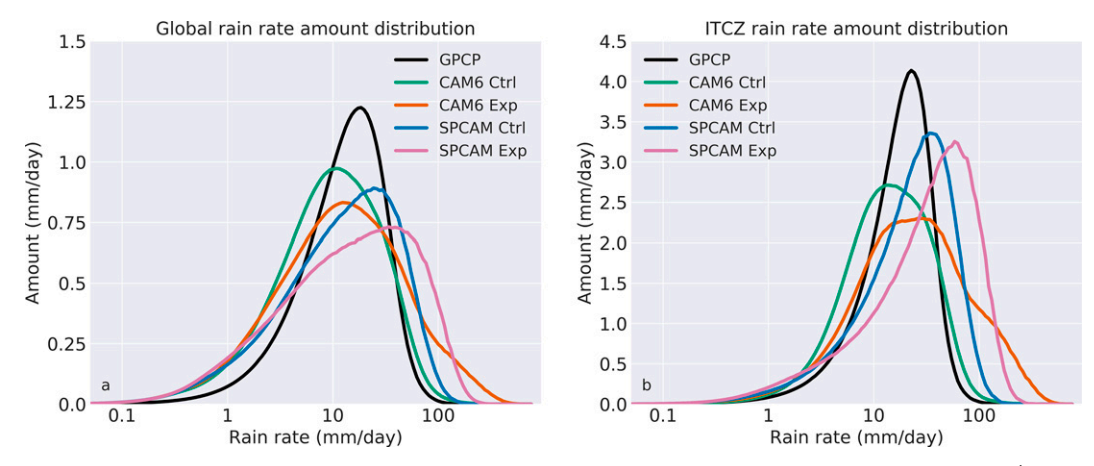


FIG. 12. Rain-rate amount distribution for (left) global and (right) the ITCZ region (where P > 5 mm day⁻¹ in the latitude range of 20°S–20°N). The ITCZ region is determined for each simulation and observational dataset using that dataset's precipitation field. The curves denote the CAM6 control (green), the CAM6 experiment (orange), the SPCAM control (blue), the SPCAM experiment (pink), and the GPCP observation-based data product (black).

many of the same regions where the LWCRE decreases (Fig. 13b). Figure 13c shows that mid- and high-level clouds over the ITCZ region decrease in amount in the sensitivity experiment relative to the control, while low clouds see an increase in amount. The total cloud fraction over the ITCZ region decreases from 78% in the control to 76% in the experiment. Over regions dominated by low clouds, the SWCRE sees enormous decreases, consistent with much brighter and/or spatially extensive low clouds, particularly just

west of the continents where stratocumulus clouds frequently occur. Low cloud amount increases in the experiment relative to the control in these regions as well (not shown), but it is unclear whether the individual clouds are also getting brighter or not. Taken together, Figs. 12 and 13 suggest that the new adjustment is particularly effective at generating resolved low clouds, which then precipitate at low rain rates. We speculate that the increase in stability discussed in the following section is at least partly responsible for the increase in low cloud

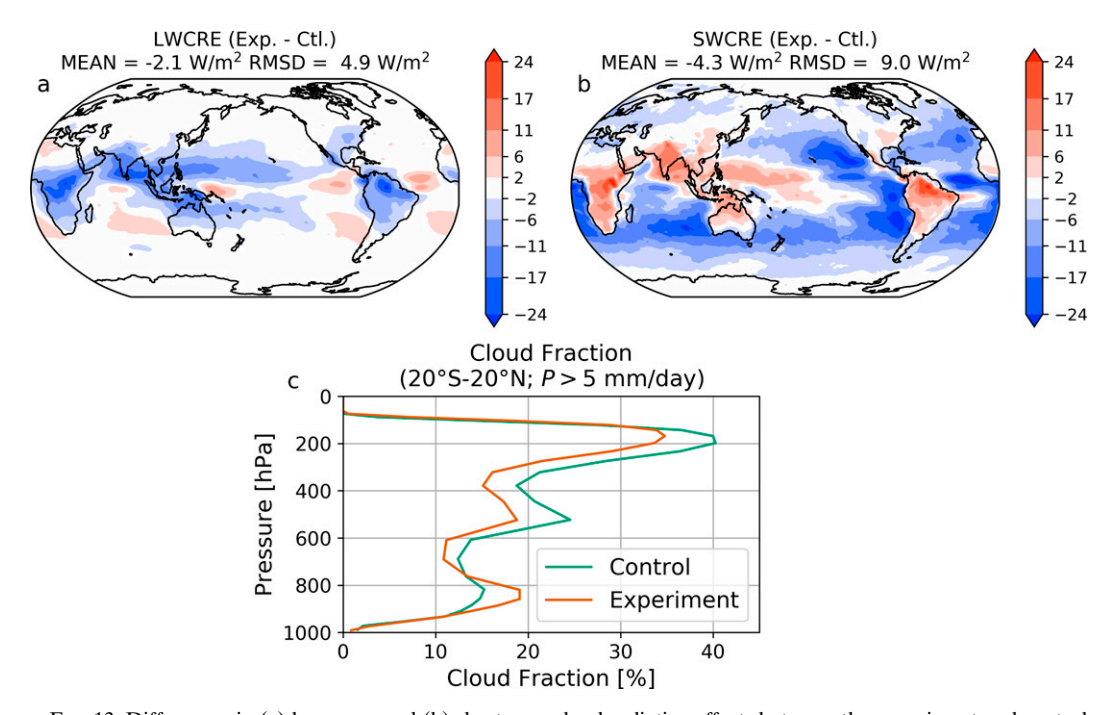


FIG. 13. Differences in (a) longwave and (b) shortwave cloud radiative effects between the experiment and control simulations; both panels have units of W m⁻². (c) Cloud fraction (%) profile averaged over the ITCZ region (where P > 5 mm day⁻¹ in the latitude range of 20°S–20°N).

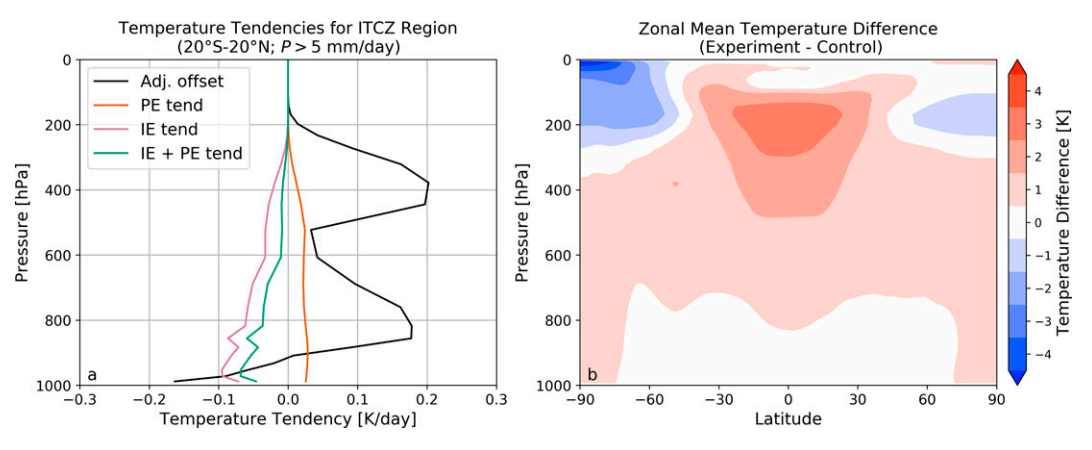


FIG. 14. (a) Energy tendency associated with the dry mass and vapor adjustment for the control simulation. (b) The zonal-mean temperature response (experiment minus control) as a function of latitude and pressure.

reflectance. The LWCRE and SWCRE patterns agree with the rainfall changes showing an increase in rainfall over the oceans and a decrease over land.

d. Physical perspective of sensitivity experiment

It is worth exploring why the adjustment increases the variability in precipitation the way it does. To do this, we examine the vertical profile of the adjustment tendency. This was not output directly from the model, but instead is computed using the climatological values of temperature, winds, and $\partial q_v/\partial t_{\rm physics}$ with Eq. (14). When these climatological values are vertically integrated, the tendency closely matches the true adjustment tendency shown in Fig. 2c for the control case (the errors are less than 1% over tropical ocean regions where $\Phi_s=0$; not shown), suggesting that the covariance between the enthalpy and kinetic energy terms of the column and the change in water vapor is small compared to the mean terms.

Figure 14a shows the profile of the adjustment tendency offset needed to conserve energy locally as diagnosed for the control simulation averaged over the ITCZ region. The diagnosed heating is roughly equal to what is applied in the sensitivity experiment—the exact value will be slightly different owing to changes in rainfall and temperature between the two simulations.

The vertical structure of the adjustment offset tendency has two peaks: one in the lower troposphere (near 800 hPa) and one in the upper troposphere (near 400 hPa). This apparent heating (relative to the control) that gets added back to balance the adjustment energy tendency in the experiment gets added after all of the physics parameterizations operate and right before the dynamics is called. As a result, this apparent heating is allowed to alter the circulation of the atmosphere before any additional physics parameterizations can act on that state. The heating leads to an increase in stability (Fig. 14b). The dry static stability $(\partial \theta/\partial z)$ increases throughout the free troposphere with maximum increases of ~20% near 800 and 300 hPa (not shown), which inhibits weaker convection from creating rainfall. Taken together with the flattening of the rainfall histogram seen in Fig. 12, the increase in precipitation variance in Fig. 10, and the cloud response in Fig. 13, these results suggest that the atmosphere is stable to

weak convection and shifts into a regime favoring more intense, but less frequent deep convection and frequent shallow convection in the experiment simulation.

The sensitivity experiment using the local energy fixer highlights the sensitivity of the simulated water cycle to the model's energy budget. Recall that the local energy fixer is not considered an ideal "fix" for the model. As outlined in section 3d, the assumption underpinning the local energy fixer is that condensed species of water have no energy, which is clearly not physically realistic. As noted in the introduction of this manuscript, the enthalpy flux from rain over the tropical west Pacific can account for 15%–60% of the net surface heat flux for precipitation events (Anderson et al. 1998). To ignore that heat flux opens the potential for large errors associated with precipitating features. Therefore, instead of considering this local energy fixer sensitivity experiment as a fix for CAM6, we highlight its use as an example for the potential impacts changes in the energy budget can have on simulated rainfall, particularly in the tropics.

Another important consideration with respect to the local energy fixer sensitivity experiment is whether it is likely to overestimate the sensitivity of the model relative to more realistic fixes, such as updating the enthalpy and including the condensates in the energy budget (section 3c). To that end, we compare the temperature tendencies imposed by our adjustment offset with the atmospheric heating and cooling associated with falling hydrometeors discussed in section 3c. Figure 14a shows the heating from potential energy loss (orange line), cooling from the hydrometeor temperature equilibrating with its environment (pink line), and their sum (green line). The main consequence with comparing the temperature tendency from the adjustment offset (the local energy fixer) with the net hydrometeor cooling is that the hydrometeor cooling does not have the strong peaks in the vertical seen in the adjustment offset. With respect to the changing stability, the lower-tropospheric cooling from hydrometeors suggests there could be an increase in stability relative to the default CAM6 configuration, although it is unlikely to be quite as strong as the stability change between the local energy fixer sensitivity experiment relative to the control CAM6. Since the hydrometeor cooling, like the adjustment offset, is largest in regions of heavy rainfall, it also has the potential to impact tropical rainfall variability. Again though, the smaller magnitude of the hydrometeor cooling relative to the adjustment offset would suggest that rainfall variability differences are likely to be less dramatic than those between the sensitivity experiment and the control.

5. Conclusions

The mass adjustment procedure used in CAM6 to conserve dry air mass exposes an inconsistency in how water is treated for the energy budget. We showed in section 2 that the inconsistency arises from including the mass of water vapor in the energy budget, but not that of condensed forms of water. Water in the vapor phase has thermal, kinetic, and potential energy, but when that vapor condenses its energy is no longer tracked by the atmosphere model, and instead of being passed to other component models, it is offset by a global fixer. The adjustment energy tendency is not globally uniform, meaning it still has a large regional energy tendency pattern with no associated flux of energy into or out of the atmosphere, violating the divergence theorem locally and possibly introducing errors to the energy budgets of the other components (ocean, ice, and land).

In section 3, we described several possible changes that could be made to allow CAM6 to satisfy the divergence theorem locally. Broadly, these options are modifying the surface flux to balance the atmospheric tendency or adjust the atmospheric energy tendency to balance the current surface plus top-ofatmosphere fluxes. The most realistic option involves relaxing assumptions made in CAM6's enthalpy formulation-specifically an enthalpy treatment that includes condensed water species and varies latent heats with temperature. Such a change to the enthalpy used in the atmosphere would necessitate including additional terms in surface enthalpy fluxes and accounting for that budget in the other component models to maintain energy conservation within the whole earth system. Offline calculations with a realistic enthalpy variable show a very different column energy tendency than that associated with the mass adjustment. In regions of precipitation, the atmosphere would experience more cooling than is currently predicted owing to the warming of hydrometeors as they fall through the atmosphere.

While using an enthalpy variable that includes all phases of water is more realistic, it is unfortunately a technical challenge beyond the scope of the current manuscript. Instead, as a first test to gauge which aspects of the simulated climate are most sensitive to assumptions in the CAM6 energy budget and the regional pattern of the adjustment energy tendency, we run a sensitivity experiment where the column energy tendency is adjusted to match the fluxes into and out of the atmosphere. This sensitivity test demonstrated that the model hydrologic cycle is extremely sensitive to assumptions regarding water's treatment in the energy budget. Precipitation, particularly its variability, shows large changes in the tropics between the sensitivity and control experiments. Compared to the control, the sensitivity experiment shows an invigoration of moist Kelvin waves and the Madden-Julian oscillation. These effects are robust in that they are reproduced in both a conventionally parameterized as well as a superparameterized version of CAM. They are also

profound in that the changes to equatorial wave activity rival those of superparameterization itself.

Given the growing movement toward using energetic frameworks to study the regional circulations that control the spatial pattern of the hydrologic cycle (Biasutti et al. 2018; Byrne et al. 2018) careful diagnosis of regional energy budgets is becoming ever more critical. Any analysis of the regional energy budget for CAM6 requires accounting for the energy tendency associated with the mass adjustment process. It is likely that other models contain the same or similar issues. For example, the atmosphere component of the Energy Exascale Earth System Model (Golaz et al. 2019; Rasch et al. 2019), which started as a fork of CAM5, has the same adjustment energy tendency. Many other models may have similar issues as well, but detailed knowledge of their energy budgets is beyond the expertise of the authors. We reached out to developers for the NASA GISS, GFDL CM4, and NorESM models. NASA GISS does not incorporate water (vapor or otherwise) into the mass used in the thermodynamic budget, so are not subject to this same issue, although this may change in future versions (G. Schmidt 2021, personal communication). The atmospheric component of CM4 includes all phases of water in its thermodynamic budget (L. Harris 2021, personal communication). In coupled mode, however, the enthalpy of water is not passed from the atmosphere to the ocean, and instead the ocean model makes its own assumptions about the incoming enthalpy of water at the surface (A. Adcroft 2021, personal communication). Modifications to the adjustment have been implemented with NorCAM (a fork of CAM used in the NorESM1-F and NorESM2 models; Guo et al. 2019; Seland et al. 2020) to account for the adjustment energy tendency with a surface enthalpy flux with only small changes in the annual mean rainfall (Guo et al. 2019). The NorCAM model also accounts for adiabatic cooling by the atmosphere as a result of the decreasing pressure from the condensation of water vapor; what they term the hydrostatic pressure work (T. Toniazzo 2021, personal communication). We hope the findings of this work encourage model development teams to explore the impacts of more rigorous energy treatments on atmospheric and coupled Earth system models.

Acknowledgments. This study is supported by the U.S. Department of Energy Office of Science Biological and Environmental Research (BER) as part of the Regional and Global Model Analysis program area. The Pacific Northwest National Laboratory (PNNL) is operated for DOE by Battelle Memorial Institute under Contract DE-AC05-76RLO1830. MSP acknowledges co-funding from NSF (AGS-1912134) and computational support from the Extreme Science and Engineering Discovery Environment supported by NSF Grant ACI-1548562 (charge number TG-ATM190002). The data were produced using resources of the National Energy Research Scientific Computing Center, a DOE Office of Science User Facility supported by the Office of Science of the U.S. Department of Energy under Contract DE-AC02-05CH11231. Figures 8 and 9 were generated in part using E3SM Diags (details here: https://e3sm.org/resources/

tools/diagnostic-tools/e3sm-diagnostics). NCO (Zender 2008) was used to generate climatologies. The authors also thank Jihyeon Jang, William Skamarock, Colin Zarzycki, Peter Blossey, Christopher Bretherton, Heng Xiao, Philip Rasch, Oksana Guba, Mark Taylor, Gavin Schmidt, Lucas Harris, Alistair Adcroft, and Thomas Toniazzo for helpful conversations.

Data availability statement. The CESM project is supported primarily by the National Science Foundation. Instructions to download the CESM code can be found here: http://www.cesm.ucar.edu/models/cesm2/release_download.html. The model output from this study may be found here: https://portal.nersc.gov/archive/home/b/beharrop/www/cam6_adjustment_data.

APPENDIX A

Enthalpy Formulations

We begin by formulating expressions for enthalpy, h, for dry air and all three phases of water:

$$h_d = c_{pd}(T - T_R) + h_{d0},$$
 (A1)

$$h_v = c_{pv}(T - T_R) + h_{v0},$$
 (A2)

$$h_l = c_l(T - T_R) + h_{l0},$$
 (A3)

$$h_i = c_i(T - T_R) + h_{i0}.$$
 (A4)

Subscript d refers to dry air, v to water vapor, l to liquid water, and i to ice water; T_R is a reference temperature, in this case, the melting temperature 273.16 K. The "0" subscript refers to the enthalpy constant for each species. It is common practice to assume the dry enthalpy constant is zero for convenience. The enthalpy constants for the three phases of water are related to one another, such that only one of h_{v0} , h_{l0} , or h_{i0} needs to be chosen and the other two can be solved for using Kirchoff's equations:

$$L_{\nu}(T) \equiv h_{\nu} - h_{l} = L_{\nu}(T_{R}) + (c_{p\nu} - c_{l})(T - T_{R}),$$
 (A5)

$$L_f(T) \equiv h_l - h_i = L_f(T_R) + (c_l - c_i)(T - T_R),$$
 (A6)

$$L_s(T) \equiv h_v - h_i = L_s(T_R) + (c_{pv} - c_i)(T - T_R).$$
 (A7)

To be consistent with the column energy formulation notation used by CAM6, we set $h_{d0} = h_{i0} = 0$ and use Eqs. (A6) and (A7) to solve for h_{t0} and h_{l0} :

$$c_{l}(T - T_{R}) + h_{l0} - c_{i}(T - T_{R}) - h_{i0}$$

$$= L_{f}(T_{R}) + (c_{l} - c_{i})(T - T_{R}),$$

$$h_{l0} = L_{f}(T_{R}),$$
(A8)

$$c_{pv}(T - T_R) + h_{v0} - c_i(T - T_R) - h_{i0}$$

$$= L_s(T_R) + (c_{pv} - c_i)(T - T_R),$$

$$h_{v0} = L_s(T_R).$$
(A9)

The total enthalpy is the mass-weighted sum of the individual enthalpies:

$$h = (1 - q_T)h_d + q_v h_v + q_l h_l + q_i h_i,$$

$$h = [(1 - q_T)c_{pd} + q_v c_{pv} + q_l c_l + q_i c_i](T - T_R) + q_v L_s(T_R) + q_l L_f(T_R).$$
(A10)

While Eq. (A10) is more rigorous than the enthalpy formulation used in CAM6, it is still subject to its own set of assumptions, most notable that the system is always in thermal equilibrium, which may not hold for falling hydrometeors. We have also assumed that the specific heat terms are all constant. Raymond (2013) note that assuming c_i is constant is a poor assumption, but the mixing ratios of ice tend to be so low that it is unlikely to have much influence on the calculations. In light of the issues presented in this manuscript, it may be worthwhile to challenge these assumptions, but we leave that for future efforts.

In Mayer et al. (2017), their expression for enthalpy is (converting their notation to match our own)

$$h = (1 - q_T)c_{pd}(T - T_R) + q_T c_l(T - T_R) + L_v(T)q_v - L_f(T)q_i + q_T h_0,$$
(A11)

where h_0 is the enthalpy constant for water, equivalent to that of liquid water at the reference temperature, T_R , such that the enthalpy of water is zero for ice at 0 K [i.e., $h_0 = c_i T_R + L_f(T_R)$]. If we change the enthalpy constant, h_0 , used by Mayer et al. (2017) to $h_0 = L_f(T_R)$, then it can be shown easily that this form of enthalpy is equivalent to Eq. (A10):

$$h = (1 - q_T)c_{pd}(T - T_R) + q_Tc_l(T - T_R) + L_v(T)q_v - L_f(T)q_i + q_TL_f(T_R),$$

$$h = (1 - q_T)c_{pd}(T - T_R) + (q_v + q_l + q_i)c_l(T - T_R) + L_v(T_R)q_v$$

$$+ q_v(c_{pv} - c_l)(T - T_R) - L_f(T_R)q_i - q_i(c_l - c_i)(T - T_R) + (q_v + q_l + q_i)L_f(T_R),$$

$$h = (1 - q_T)c_{pd}(T - T_R) + (q_l)c_l(T - T_R) + L_v(T_R)q_v + q_v(c_{pv})(T - T_R)$$

$$+ q_i(c_i)(T - T_R) + q_vL_f(T_R) + q_lL_f(T_R),$$

$$h = [(1 - q_T)c_{pd} + q_vc_{pv} + q_lc_l + q_ic_l](T - T_R) + q_vL_s(T_R) + q_lL_f(T_R).$$
(A12)

For completeness, the following values for constants are used in CAM6 and the analyses presented within this manuscript.

$$c_{pd} = 1004.64 \,\mathrm{J} \,\mathrm{kg}^{-1} \,\mathrm{K}^{-1},$$

$$c_{pv} = 1810.0 \,\mathrm{J} \,\mathrm{kg}^{-1} \,\mathrm{K}^{-1},$$

$$c_{l} = 4188.0 \,\mathrm{J} \,\mathrm{kg}^{-1} \,\mathrm{K}^{-1},$$

$$c_{i} = 2117.27 \,\mathrm{J} \,\mathrm{kg}^{-1} \,\mathrm{K}^{-1},$$

$$L_{v}(T_{R}) = 2501 \,000.0 \,\mathrm{J} \,\mathrm{kg}^{-1},$$

$$L_{f}(T_{R}) = 333 \,700.0 \,\mathrm{J} \,\mathrm{kg}^{-1},$$

$$L_{s}(T_{R}) = 2834 \,700.0 \,\mathrm{J} \,\mathrm{kg}^{-1},$$

$$T_{R} = 273.16 \,\mathrm{K}.$$
(A13)

APPENDIX B

Adjustment of Temperature

We want to formulate an expression for the adjustment that conserves the column energy [Eq. (12)]. Since the two latent terms in Eq. (12) are already conserved during the adjustment, we focus on the thermal and kinetic energy terms. Note that we are not accounting for the energy tendency related to the surface pressure term, $p_s\Phi_s/g$. The surface geopotential is zero over oceans, and where it is nonzero, the surface pressure changes owing to the water vapor tendency in the column tend to be small. Hence, ignoring this term is an acceptable approximation for the purposes of this study, as shown in Fig. 7.

Conserving the thermal energy term, $c_{pd}T\delta p/g$, requires an expression modifying temperature to offset the changes from δp . In other words we require, following the notation of Neale et al. (2012) section 3.1.8,

$$c_{pd}T_{n+1}^k \frac{\delta^k p_{n+1}}{g} = c_{pd}T_{n^*}^k \frac{\delta^k p_n}{g},$$
 (B1)

where δp is the pressure thickness of a layer, superscript k refers to the model layer, subscript n refers to the state before the physics tendencies are applied, subscript n^* refers to the state after the physics tendencies have been applied but before the adjustment, subscript n+1 refers to the state after the adjustment, and all other symbols are the same as in the body of the manuscript. From Eq. (B1), we see that to enforce thermal energy conservation, we require

$$T_{n+1}^k = T_{n^*}^k \frac{\delta^k p_n}{\delta^k p_{n+1}}.$$
 (B2)

From Eq. (3.64) of Neale et al. (2012) we have

$$\frac{\delta^k p_n}{\delta^k p_{n+1}} = \left(1 - q_{v,n}^k + q_{v,n^*}^k\right)^{-1}.$$
 (B3)

Therefore, the adjustment update to temperature may be written as

$$T_{n+1}^k = \frac{T_{n^*}^k}{1 - q_{nn}^k + q_{nn^*}^k}.$$
 (B4)

Note that this is the same scaling factor that is applied to humidity [see Eq. (3.65) of Neale et al. 2012]. A similar equation is used for the kinetic energy. It is worth noting that the release version of CESM2.1.0 has code in place for updating the static and kinetic energy budget terms that agree with the adjustments derived here, though they use an inconsistent form of energy [for more discussion on the correct energy usage in CAM, see Williamson et al. (2015)] and are off by default.

REFERENCES

Adam, O., T. Bischoff, and T. Schneider, 2016: Seasonal and interannual variations of the energy flux equator and ITCZ. Part I: Zonally averaged ITCZ position. *J. Climate*, 29, 7281–7293, https://doi.org/10.1175/JCLI-D-15-0710.1.

Adler, R. F., and Coauthors, 2003: The version-2 Global Precipitation Climatology Project (GPCP) monthly precipitation analysis (1979–present). J. Hydrometeor., 4, 1147–1167, https://doi.org/10.1175/1525-7541(2003)004<1147: TVGPCP>2.0.CO;2.

Anderson, S. P., A. Hinton, and R. A. Weller, 1998: Moored observations of precipitation temperature. *J. Atmos. Oceanic Technol.*, 15, 979–986, https://doi.org/10.1175/1520-0426(1998) 015<0979:MOOPT>2.0.CO;2.

Back, L. E., and C. S. Bretherton, 2006: Geographic variability in the export of moist static energy and vertical motion profiles in the tropical Pacific. *Geophys. Res. Lett.*, 33, L17810, https:// doi.org/10.1029/2006GL026672.

Benedict, J. J., and D. A. Randall, 2009: Structure of the Madden–Julian oscillation in the superparameterized CAM. *J. Atmos. Sci.*, **66**, 3277–3296, https://doi.org/10.1175/2009JAS3030.1.

Biasutti, M., and Coauthors, 2018: Global energetics and local physics as drivers of past, present and future monsoons. *Nat. Geosci.*, 11, 392–400, https://doi.org/10.1038/s41561-018-0137-1.

Bogenschutz, P. A., A. Gettelman, H. Morrison, V. E. Larson, C. Craig, and D. P. Schanen, 2013: Higher-order turbulence closure and its impact on climate simulations in the Community Atmosphere Model. J. Climate, 26, 9655–9676, https:// doi.org/10.1175/JCLI-D-13-00075.1.

Boos, W. R., and R. L. Korty, 2016: Regional energy budget control of the intertropical convergence zone and application to mid-Holocene rainfall. *Nat. Geosci.*, 9, 892–897, https://doi.org/10.1038/ngeo2833.

Bosilovich, M. G., F. R. Robertson, and J. Chen, 2011: Global energy and water budgets in MERRA. *J. Climate*, **24**, 5721–5739, https://doi.org/10.1175/2011JCLI4175.1.

Byers, H. R., H. Moses, and P. J. Harney, 1949: Measurement of rain temperature. J. Meteor., 6, 51–55, https://doi.org/10.1175/ 1520-0469(1949)006<0051:MORT>2.0.CO;2.

Byrne, M. P., and T. Schneider, 2016: Narrowing of the ITCZ in a warming climate: Physical mechanisms. *Geophys. Res. Lett.*, **43**, 11 350–11 357, https://doi.org/10.1002/2016GL070396.

—, A. G. Pendergrass, A. D. Rapp, and K. R. Wodzicki, 2018: Response of the intertropical convergence zone to climate

- change: Location, width, and strength. *Curr. Climate Change Rep.*, **4**, 355–370, https://doi.org/10.1007/s40641-018-0110-5.
- Catry, B., J. F. Geleyn, M. Tudor, P. Bénard, and A. Trojáková, 2007: Flux-conservative thermodynamic equations in a massweighted framework. *Tellus*, **59A**, 71–79, https://doi.org/10. 1111/j.1600-0870.2006.00212.x.
- Danabasoglu, G., and Coauthors, 2020: The Community Earth System Model version 2 (CESM2). *J. Adv. Model. Earth Syst.*, **12**, e2019MS001916, https://doi.org/10.1029/2019MS001916.
- Degrauwe, D., Y. Seity, F. Bouyssel, and P. Termonia, 2016: Generalization and application of the flux-conservative thermodynamic equations in the AROME model of the ALADIN system. *Geosci. Model Dev.*, **9**, 2129–2142, https://doi.org/10.5194/gmd-9-2129-2016.
- DeMaria, M., 1985: Linear response of a stratified tropical atmosphere to convective forcing. *J. Atmos. Sci.*, **42**, 1944–1959, https://doi.org/10.1175/1520-0469(1985)042<1944: LROAST>2.0.CO;2.
- DeMott, C. A., D. A. Randall, and M. Khairoutdinov, 2007: Convective precipitation variability as a tool for general circulation model analysis. *J. Climate*, 20, 91–112, https://doi.org/10.1175/JCLI3991.1.
- Frierson, D. M. W., and Coauthors, 2013: Contribution of ocean overturning circulation to tropical rainfall peak in the Northern Hemisphere. *Nat. Geosci.*, 6, 940–944, https://doi.org/10. 1038/ngeo1987.
- Gettelman, A., and H. Morrison, 2015: Advanced two-moment bulk microphysics for global models. Part I: Off-line tests and comparison with other schemes. *J. Climate*, 28, 1268–1287, https://doi.org/10.1175/JCLI-D-14-00102.1.
- Golaz, J.-C., V. E. Larson, and W. R. Cotton, 2002: A PDF-based model for boundary layer clouds. Part I: Method and model description. J. Atmos. Sci., 59, 3540–3551, https://doi.org/10. 1175/1520-0469(2002)059<3540:APBMFB>2.0.CO;2.
- —, and Coauthors, 2019: The DOE E3SM coupled model version 1: Overview and evaluation at standard resolution. J. Adv. Model. Earth Syst., 11, 2089–2129, https://doi.org/10.1029/2018MS001603.
- Gosnell, R., C. W. Fairall, and P. J. Webster, 1995: The sensible heat of rainfall in the tropical ocean. J. Geophys. Res., 100, 18437, https://doi.org/10.1029/95JC01833.
- Grabowski, W. W., 2001: Coupling cloud processes with the large-scale dynamics using the clouds-resolving convection parameterization (CRCP). J. Atmos. Sci., 58, 978–997, https://doi.org/10.1175/1520-0469(2001)058<0978:CCPWTL>2.0.CO;2.
- —, and P. K. Smolarkiewicz, 1999: CRCP: A cloud resolving convection parameterization for modeling the tropical convecting atmosphere. *Physica D*, **133**, 171–178, https://doi.org/ 10.1016/S0167-2789(99)00104-9.
- Guo, C., M. Bentsen, I. Bethke, M. Ilicak, J. Tjiputra, T. Toniazzo, J. Schwinger, and O. Helge Otterä, 2019: Description and evaluation of NorESM1-F: A fast version of the Norwegian Earth System Model (NorESM). *Geosci. Model Dev.*, 12, 343–362, https://doi.org/10.5194/gmd-12-343-2019.
- Harrop, B. E., J. Lu, and L. R. Leung, 2019: Sub-cloud moist entropy curvature as a predictor for changes in the seasonal cycle of tropical precipitation. *Climate Dyn.*, 53, 3463–3479, https://doi.org/10.1007/s00382-019-04715-2.
- Hartmann, D. L., H. H. Hendon, and R. A. Houze, 1984: Some implications of the mesoscale circulations in tropical cloud clusters for large-scale dynamics and climate. *J. Atmos. Sci.*, 41, 113–121, https://doi.org/10.1175/1520-0469(1984)041<0113: SIOTMC>2.0.CO;2.

- Huffman, G. J., and D. T. Bolvin, 2013a: GPCP version 2.2 SG combined precipitation data set documentation. NASA GSFC Doc., 46 pp., https://iridl.ldeo.columbia.edu/documentation/NASA/GPCP/V2p2/V2.2_doc.pdf.
- —, and —, 2013b: Version 1.2 GPCP one-degree daily precipitation data set documentation. NASA, Goddard Space Flight Center, 27 pp., https://www1.ncdc.noaa.gov/pub/data/gpcp/daily-v1.2/documentation/1DD_v1.2_doc.pdf (for the actual data, see https://doi.org/10.5065/D6D50K46).
- R. F. Adler, M. M. Morrissey, D. T. Bolvin, S. Curtis, R. Joyce, B. McGavock, and J. Susskind, 2001: Global precipitation at one-degree daily resolution from multisatellite observations. *J. Hydrometeor.*, 2, 36–50, https://doi.org/10. 1175/1525-7541(2001)002<0036:GPAODD>2.0.CO;2.
- —, and Coauthors, 2007: The TRMM Multisatellite Precipitation Analysis (TMPA): Quasi-global, multiyear, combined-sensor precipitation estimates at fine scales. *J. Hydrometeor.*, 8, 38–55, https://doi.org/10.1175/JHM560.1.
- Iacono, M. J., J. S. Delamere, E. J. Mlawer, M. W. Shephard, S. A. Clough, and W. D. Collins, 2008: Radiative forcing by long-lived greenhouse gases: Calculations with the AER radiative transfer models. J. Geophys. Res., 113, D13103, https:// doi.org/10.1029/2008JD009944.
- Igel, M. R., and A. L. Igel, 2018: The energetics and magnitude of hydrometeor friction in clouds. J. Atmos. Sci., 75, 1343–1350, https://doi.org/10.1175/JAS-D-17-0285.1.
- Inoue, K., and L. E. Back, 2017: Gross moist stability analysis: Assessment of satellite-based products in the GMS plane. J. Atmos. Sci., 74, 1819–1837, https://doi.org/10.1175/JAS-D-16-0218.1.
- Kang, S. M., D. M. W. Frierson, and I. M. Held, 2009: The tropical response to extratropical thermal forcing in an idealized GCM: The importance of radiative feedbacks and convective parameterization. *J. Atmos. Sci.*, 66, 2812–2827, https://doi.org/10.1175/2009JAS2924.1.
- Kasahara, A., 1974: Various vertical coordinate systems used for numerical weather prediction. *Mon. Wea. Rev.*, **102**, 509–522, https://doi.org/10.1175/1520-0493(1974)102<0509: VVCSUF>2.0.CO;2.
- Khairoutdinov, M. F., and D. A. Randall, 2001: A cloud resolving model as a cloud parameterization in the NCAR Community Climate System model: Preliminary results. *Geophys. Res. Lett.*, 28, 3617–3620, https://doi.org/10.1029/2001GL013552.
- —, —, and C. DeMott, 2005: Simulations of the atmospheric general circulation using a cloud-resolving model as a superparameterization of physical processes. *J. Atmos. Sci.*, **62**, 2136–2154, https://doi.org/10.1175/JAS3453.1.
- Kinzer, G. D., and R. Gunn, 1951: The evaporation, temperature and thermal relaxation-time of freely falling waterdrops. J. Meteor., 8, 71–83, https://doi.org/10.1175/1520-0469(1951)008<0071:TETATR>2.0.CO;2.
- Kooperman, G. J., M. S. Pritchard, M. A. Burt, M. D. Branson, and D. A. Randall, 2016: Robust effects of cloud superparameterization on simulated daily rainfall intensity statistics across multiple versions of the Community Earth System Model. J. Adv. Model. Earth Syst., 8, 140–165, https://doi.org/ 10.1002/2015MS000574.
- Laprise, R., and C. Girard, 1990: A spectral general circulation model using a piecewise-constant finite-element representation on a hybrid vertical coordinate system. *J. Climate*, 3, 32–52, https://doi.org/10.1175/1520-0442(1990)003<0032: ASGCMU>2.0.CO;2.

- Lauritzen, P. H., and D. L. Williamson, 2019: A total energy error analysis of dynamical cores and physics-dynamics coupling in the Community Atmosphere Model (CAM). J. Adv. Model. Earth Syst., 11, 1309–1328, https://doi.org/10.1029/ 2018MS001549.
- Lin, S.-J., and R. B. Rood, 1996: Multidimensional flux-form semi-Lagrangian transport schemes. *Mon. Wea. Rev.*, **124**, 2046–2070, https://doi.org/10.1175/1520-0493(1996)124<2046: MFFSLT>2.0.CO;2.
- —, and —, 1997: An explicit flux-form semi-Lagrangian shallow-water model on the sphere. *Quart. J. Roy. Meteor. Soc.*, **123**, 2477–2498, https://doi.org/10.1002/qj.49712354416.
- Liu, X., P. L. Ma, H. Wang, S. Tilmes, B. Singh, R. C. Easter, S. J. Ghan, and P. J. Rasch, 2016: Description and evaluation of a new four-mode version of the Modal Aerosol Module (MAM4) within version 5.3 of the Community Atmosphere Model. *Geosci. Model Dev.*, 9, 505–522, https://doi.org/10. 5194/gmd-9-505-2016.
- Lu, J., D. Xue, L. R. Leung, F. Liu, F. Song, B. Harrop, and W. Zhou, 2021: The leading modes of Asian summer monsoon variability as pulses of atmospheric energy flow. *Geophys. Res. Lett.*, 48, e2020GL091629, https://doi.org/10.1029/ 2020GL091629.
- Mayer, M., L. Haimberger, J. M. Edwards, and P. Hyder, 2017: Toward consistent diagnostics of the coupled atmosphere and ocean energy budgets. *J. Climate*, 30, 9225–9246, https://doi. org/10.1175/JCLI-D-17-0137.1.
- Mitchell, T. D., and P. D. Jones, 2005: An improved method of constructing a database of monthly climate observations and associated high-resolution grids. *Int. J. Climatol.*, 25, 693–712, https://doi.org/10.1002/joc.1181.
- Mlawer, E. J., S. J. Taubman, P. D. Brown, M. J. Iacono, and S. A. Clough, 1997: Radiative transfer for inhomogeneous atmospheres: RRTM, a validated correlated-k model for the longwave. J. Geophys. Res., 102, 16663–16682, https://doi. org/10.1029/97JD00237.
- Neale, R. B., and Coauthors, 2012: Description of the NCAR Community Atmosphere Model (CAM 5.0). NCAR Tech. Note NCAR Tech. Note NCAR/TN-486+ STR, 274 pp., www.cesm. ucar.edu/models/cesm1.0/cam/docs/description/cam5_desc.pdf.
- New, M., M. Hulme, and P. Jones, 1999: Representing twentieth-century space–time climate variability. Part I: Development of a 1961–90 mean monthly terrestrial climatology. *J. Climate*, 12, 829–856, https://doi.org/10.1175/1520-0442(1999)012<0829: RTCSTC>2.0.CO;2.
- Pauluis, O., and I. M. Held, 2002: Entropy budget of an atmosphere in radiative-convective equilibrium. Part II: Latent heat transport and moist processes. *J. Atmos. Sci.*, **59**, 140–149, https://doi.org/10.1175/1520-0469(2002)059<0140: EBOAAI>2.0.CO;2.
- —, and J. Dias, 2012: Satellite estimates of precipitationinduced dissipation in the atmosphere. *Science*, 335, 953–956, https://doi.org/10.1126/science.1215869.
- —, V. Balaji, and I. M. Held, 2000: Frictional dissipation in a precipitating atmosphere. J. Atmos. Sci., 57, 989–994, https:// doi.org/10.1175/1520-0469(2000)057<0989:FDIAPA>2.0.CO;2.
- Pendergrass, A. G., and D. L. Hartmann, 2014: Two modes of change of the distribution of rain. J. Climate, 27, 8357–8371, https://doi.org/10.1175/JCLI-D-14-00182.1.
- Randall, D., M. Khairoutdinov, A. Arakawa, and W. Grabowski, 2003: Breaking the cloud parameterization deadlock. *Bull. Amer. Meteor. Soc.*, 84, 1547–1564, https://doi.org/10.1175/BAMS-84-11-1547.

- Rasch, P. J., and Coauthors, 2019: An overview of the atmospheric component of the energy exascale Earth system model. J. Adv. Model. Earth Syst., 11, 2377–2411, https://doi.org/10.1029/2019MS001629.
- Raymond, D. J., 2013: Sources and sinks of entropy in the atmosphere. J. Adv. Model. Earth Syst., 5, 755–763, https://doi.org/10.1002/jame.20050.
- Romps, D. M., 2008: The dry-entropy budget of a moist atmosphere. J. Atmos. Sci., 65, 3779–3799, https://doi.org/10.1175/2008JAS2679.1.
- Sabuwala, T., G. Gioia, and P. Chakraborty, 2015: Effect of rainpower on hurricane intensity. *Geophys. Res. Lett.*, 42, 3024–3029, https://doi.org/10.1002/2015GL063785.
- Schumacher, C., R. A. Houze, and I. Kraucunas, 2004: The tropical dynamical response to latent heating estimates derived from the TRMM Precipitation Radar. J. Atmos. Sci., 61, 1341–1358, https://doi.org/10.1175/1520-0469(2004)061<1341: TTDRTL>2.0.CO:2.
- Seland, Ø., and Coauthors, 2020: Overview of the Norwegian Earth System Model (NorESM2) and key climate response of CMIP6 DECK, historical, and scenario simulations. *Geo-sci. Model Dev.*, 13, 6165–6200, https://doi.org/10.5194/gmd-13-6165-2020.
- Stull, R., 2011: Wet-bulb temperature from relative humidity and air temperature. J. Appl. Meteor. Climatol., 50, 2267–2269, https://doi.org/10.1175/JAMC-D-11-0143.1.
- Takacs, L. L., M. J. Suárez, and R. Todling, 2016: Maintaining atmospheric mass and water balance in reanalyses. *Quart J. Roy. Meteor. Soc.*, **142**, 1565–1573, https://doi.org/10.1002/qj. 2763
- Trenberth, K. E., 1997: Using atmospheric budgets as a constraint on surface fluxes. *J. Climate*, **10**, 2796–2809, https://doi.org/10. 1175/1520-0442(1997)010<2796:UABAAC>2.0.CO;2.
- —, and J. T. Fasullo, 2018: Applications of an updated atmospheric energetics formulation. *J. Climate*, 31, 6263–6279, https://doi.org/10.1175/JCLI-D-17-0838.1.
- —, D. P. Stepaniak, and J. M. Caron, 2002: Accuracy of atmospheric energy budgets from analyses. *J. Climate*, **15**, 3343–3360, https://doi.org/10.1175/1520-0442(2002)015<3343: AOAEBF>2.0.CO;2.
- van Beek, L. P., T. Eikelboom, M. T. van Vliet, and M. F. Bierkens, 2012: A physically based model of global freshwater surface temperature. Water Resour. Res., 48, W09530, https://doi.org/10.1029/2012WR011819.
- Wheeler, M., and G. N. Kiladis, 1999: Convectively coupled equatorial waves: Analysis of clouds and temperature in the wavenumber–frequency domain. *J. Atmos. Sci.*, **56**, 374–399, https://doi.org/10.1175/1520-0469(1999)056<0374: CCEWAO>2.0.CO;2.
- Williamson, D. L., J. G. Olson, C. Hannay, T. Toniazzo, M. Taylor, and V. Yudin, 2015: Energy considerations in the Community Atmosphere Model (CAM). J. Adv. Model. Earth Syst., 7, 1178–1188, https://doi.org/10.1002/2015MS000448.
- Zender, C. S., 2008: Analysis of self-describing gridded geoscience data with netCDF operators (NCO). *Environ. Modell. Software*, 23, 1338–1342, https://doi.org/10.1016/j.envsoft.2008.03.004.
- Zhang, G. J., and N. A. McFarlane, 1995: Sensitivity of climate simulations to the parameterization of cumulus convection in the Canadian Climate Centre general circulation model. *Atmos.—Ocean*, 33, 407–446, https://doi.org/10.1080/07055900. 1995.9649539.